JOURNAL OF GUIDANCE, CONTROL, AND DYNAMICS
Vol. 31, No. 5, September–October 2008

Optimal Fuel-Balanced Impulsive Formationkeeping for Perturbed Spacecraft Orbits

Igor Beigelman* and Pini Gurfil†
Technion–Israel Institute of Technology, 32000 Haifa, Israel

DOI: 10.2514/1.34266

This paper develops an impulsive spacecraft formation-flying control algorithm using relative-orbital-element corrections. This formalism introduces an inherent freedom that is used for deriving an optimal formationkeeping law, balancing the fuel consumption among the spacecraft based on the impulsive Gauss variational equations. The main idea is that formulating the problem of formationkeeping in terms of relative-orbital-element corrections leaves the final values of the orbital elements unconstrained, thus allowing the spacecraft to create a natural energy-balanced formation. The freedom rendered by this modeling is used to find optimal impulsive maneuvers, minimizing the squared l^2-norm of the velocity-correction vector, which can be used for formation initialization and control. The optimization is solved using the least-squares method. The optimal formationkeeping method is designed to accommodate the effects of oblateness and drag. Based on graph theory, it is shown that the spacecraft will naturally form a stable energy-balanced formation and that the optimal formationkeeping strategy is invariant to the spanning tree. The algorithm is illustrated by simulating the motion of a formation of spacecraft possessing different ballistic coefficients subject to oblateness and drag.

Nomenclature

A	=	system matrix
a	=	semimajor axis
C_D	=	drag coefficient
e	=	eccentricity
f	=	true anomaly
G	=	graph
g_0	=	gravitational acceleration at sea level
H	=	cost functional
h	=	orbital angular momentum
I	=	inclination
$\mathcal{I}_n$	=	modified Bessel function of the first kind
I_{sp}	=	specific impulse
K_D	=	ballistic coefficient
M	=	mean anomaly
m	=	mass
n	=	mean motion
p	=	semilatus rectum
r	=	orbit radius
S_i	=	spacecraft i
s	=	reference area
$\boldsymbol{\alpha}$	=	classical orbital-element vector
β	=	inverse of the atmospheric scale factor
$\Delta\mathbf{v}$	=	velocity-correction vector
$\Delta(.)$	=	variation of (.)
$\boldsymbol{\lambda}$	=	Lagrange multiplier vector
μ	=	gravitational constant
Ω	=	right ascension of the ascending node
ω	=	argument of perigee
$\|\cdot\|_m$	=	m-norm of a vector

Presented as Paper 6544 at the AIAA Guidance, Navigation and Control Conference and Exhibit, Hilton Head, SC, 20–23 August 2007; received 26 August 2007; revision received 8 January 2008; accepted for publication 8 January 2008.

*Graduate Student, Faculty of Aerospace Engineering; beigel@tx.technion.ac.il.

†Senior Lecturer, Faculty of Aerospace Engineering; pgurfil@technion.ac.il. Associate Fellow AIAA.

I. Introduction

CONTROL of relative spacecraft motion, known as formationkeeping, is an enabling technology for spacecraft formation-flying missions. Modeling relative-motion dynamics, an essential infrastructure for formationkeeping, has seen significant progress in recent years, since Clohessy and Wiltshire [1] published their linearized relative-motion approximation in the early 1960s. For example, Karlgaard and Lutze [2] derived an approximate solution to second-order relative-motion equations for spacecraft in near-circular Keplerian orbits. Gurfil and Kasdin [3] presented a methodology for obtaining high-order approximations of the relative motion between spacecraft by using the Cartesian configuration space in conjunction with the classical orbital elements. Chichka [4] used the linear Clohessy–Wiltshire equations to find natural formations of satellites with a constant apparent distribution, an important application of the relative-motion equations for remote sensing.

However, natural formations may not survive, due to orbital perturbations. The need for formationkeeping, therefore, stems from the fact that space is a perturbed environment, thus inducing separation of the formation-flying spacecraft orbital planes. In low Earth orbits, the dominant perturbations are the Earth oblateness and drag, and at higher altitudes, the spacecraft are perturbed by the attraction forces of the sun and the moon.

The growing number of autonomous spacecraft missions that are to perform complicated missions in close proximity requires accurate, robust, and fuel-efficient formationkeeping algorithms. Thus, attention should be given to developing a new rigorous control approach, taking into account the effect of all dominant orbital perturbations.

One such perturbation is Earth's oblateness. Because J_2 perturbations affect the orbital elements of each spacecraft in the formation differently, the formation will tend to separate. An analytical method developed by Alfriend et al. [5] can be used to evaluate the differential forces on the formation-flying spacecraft. Moreover, Schaub and Alfriend [6] also found that J_2-invariant relative orbits can be designed analytically; spacecraft placed on the Schaub–Alfriend orbits will be influenced by the same forces and will therefore have the same drift, thus yielding bounded relative motion in the configuration space.

Formationkeeping can be implemented by using either impulsive control, relying on chemical thrusters, or continuous control, using low-thrust electric propulsion. Impulsive formationkeeping usually assumes that the orbital elements of some reference orbit are known

and attempts to generate control commands that will match the instantaneous orbital elements to some desired values [7], even under orbital perturbations [8]. However, in many cases, such as in situ field mapping and astronomical observations, setting an a priori reference orbit is not a mission requirement (although orbit knowledge is required). More important, on some occasions, specifying the reference orbit a priori can result in a greater fuel consumption.

At this point, one may ask what can be done to the improve the existing [7–10] impulsive-formationkeeping schemes. The answer is that the overall amount of propellent used for formationkeeping can be optimally distributed among the spacecraft if the reference orbit for the formation-flying spacecraft is *not* specified. In other words, if one used the relative-orbital-element corrections to define the formationkeeping strategy, the formation could be designed so that the *relative* geometry is determined without imposing an *absolute* configuration on the formation. This approach is conceptually different from existing distributed spacecraft system optimization methods [11].

Relative-orbital-element corrections are the differences between the successive corrections of orbital elements of any two formation-flying spacecraft. In essence, these elements differ from the orbital-element differences proposed by Schaub [12], because they do not depend on a particular reference orbit. The proposed modeling approach remains valid in the presence of orbital perturbations.

In this work, we develop a generic method for the impulsive control of formation-flying spacecraft using the Gauss variational equations (GVEs) [13] as the dynamic model and the classical relative-orbital-element corrections as the variables representing the formation structure. As opposed to other works [14–16], we shall not attempt to minimize the overall amount of fuel consumed by the formation-flying spacecraft, but rather to optimally balance a given amount of fuel among the spacecraft. This prevents an undesirable situation in which some of the spacecraft maneuver much more than others, thus considerably increasing the a priori propellent margin of the entire formation.

This approach relies on the key observation that formulating the problem of formationkeeping in terms of relative-orbital-element corrections leaves the final values of the corrected elements unconstrained. This freedom can be used to design optimal impulsive maneuvers for formation initialization, reconfiguration and maintenance. We show that our impulsive control scheme is a natural scheme in the sense that it creates a stable formation that corresponds to an optimum balancing of the overall amount of propellent. This approach is substantially different from other fuel-balancing methods [17], wherein the control design exploits the approximate dynamics given by the Clohessy–Wiltshire equations and an approximate perturbation model.

In our analysis, we use elementary graph theory [18] to classify the formation topologies and to guide the quest for optimal maneuvers. Graph theory is a useful tool for analyzing multiple spacecraft formations; thus far, however, it has been mostly used in the continuous-formationkeeping setting [19]. We offer to apply a graph-theory-inspired analysis for impulsive-formationkeeping design.

II. Dynamic Model

In this section, we briefly outline the underlying dynamic model used for the design of optimal formationkeeping, including the effects of J_2 and drag.

A. Coordinate Systems

We first define the following coordinate systems [20]:

1) $\mathcal{R}$ is a rotating polar coordinate system, centered at the spacecraft. The fundamental plane is the orbital plane. The unit vector $\hat{\mathbf{r}}$ is directed from the spacecraft radially outward, $\hat{\mathbf{h}}$ is normal to the fundamental plane, and $\hat{\boldsymbol{\theta}}$ completes the right-hand setup.

2) $\mathcal{T}$ is a rotating tangential-normal frame, centered at the spacecraft. The fundamental plane is the orbital plane. The unit vector $\hat{\mathbf{t}}$ lies along the spacecraft velocity vector, $\hat{\mathbf{h}}$ coincides with the instantaneous angular momentum vector, and $\hat{\mathbf{n}}$ completes the right-hand setup.

3) $\mathcal{P}$ is a perifocal coordinate system, centered at the primary. The fundamental plane is the orbital plane. The unit vector $\hat{\mathbf{x}}_p$ is directed from the primary's center to the periapsis, $\hat{\mathbf{z}}_p$ is normal to the fundamental plane, and $\hat{\mathbf{y}}_p$ completes the right-hand setup.

4) $\mathcal{I}$ is an inertial coordinate system, centered at the Earth. The fundamental plane is the equator, $\hat{\mathbf{X}}$ is directed from the Earth's center to the vernal equinox, $\hat{\mathbf{Z}}$ is normal to the fundamental plane, and $\hat{\mathbf{Y}}$ completes the right-hand setup.

B. Gauss Variational Equations

The GVEs model the effect of a control and/or a disturbance acceleration vector

$$\boldsymbol{u} = (u_t, u_n, u_h)^T$$

on the osculating orbital element's time derivatives. This vector is represented in the reference frame $\mathcal{T}$, and so u_t and u_n are the input components in the plane of the osculating orbit along the velocity vector and perpendicular to it, respectively, and u_h lies along the instantaneous angular momentum vector, normal to the orbital plane. In the case of impulsive maneuvers, we can write

$$\dot{\alpha}\Delta t = \Delta\alpha, \qquad u_t\Delta t = \Delta V_t, \qquad u_n\Delta t = \Delta V_n, \qquad u_h\Delta t = \Delta V_h \tag{1}$$

where α is an orbital element; $\Delta\alpha$ is an orbital-element correction; ΔV_t, ΔV_n, and ΔV_h are the components of the velocity-correction vector in frame $\mathcal{T}$; and the impulsive time interval $\Delta t \to 0$. The impulsive form of the GVEs defines algebraic relationships between the orbital-element corrections and the components of the velocity-correction vector [20]:

$$\Delta a = \frac{2a^2 v}{\mu}\Delta V_t \tag{2a}$$

$$\Delta e = \frac{1}{v}\left[2(e+\cos f)\Delta V_t - \frac{r}{a}\sin f\,\Delta V_n\right] \tag{2b}$$

$$\Delta I = \frac{r\cos(f+\omega)}{h}\Delta V_h \tag{2c}$$

$$\Delta\Omega = \frac{r\sin(f+\omega)}{h\sin I}\Delta V_h \tag{2d}$$

$$\Delta\omega = \frac{1}{ev}\left[2\sin f\,\Delta V_t + \left(2e + \frac{r}{a}\cos f\right)\Delta V_n\right] - \frac{r\sin(f+\omega)\cos I}{h\sin I}\Delta V_h \tag{2e}$$

$$\Delta M = -\frac{b}{eav}\left[2\left(1+\frac{e^2 r}{p}\right)\sin f\,\Delta V_t + \frac{r}{a}\cos f\,\Delta V_n\right] \tag{2f}$$

where a is the semimajor axis, e is the eccentricity, I is the inclination, Ω is the right ascension of the ascending node, ω is the argument of perigee, M is the mean anomaly, the parameter f is the true anomaly, r is the scalar orbit radius, and p is the semilatus rectum. The mean motion n satisfies $n = \sqrt{\mu/a^3}$, where μ is the gravitational parameter. The semiminor axis b satisfies $b = a\sqrt{1-e^2}$.

Consequently, in matrix form, GVEs (2) for some spacecraft S_i can be written as

$$\Delta\boldsymbol{\alpha}_i = G(\boldsymbol{\alpha}_i)\Delta\mathbf{v}_i \tag{3}$$

where

$$\Delta\boldsymbol{\alpha}_i = \begin{bmatrix} \Delta a \\ \Delta e \\ \Delta I \\ \Delta\Omega \\ \Delta\omega \\ \Delta M \end{bmatrix}_i, \qquad G(\boldsymbol{\alpha}_i) = \begin{bmatrix} \mathbf{c}_a^T \\ \mathbf{c}_e^T \\ \mathbf{c}_I^T \\ \mathbf{c}_\Omega^T \\ \mathbf{c}_\omega^T \\ \mathbf{c}_M^T \end{bmatrix}_i, \qquad \Delta\mathbf{v}_i = \begin{bmatrix} \Delta V_t \\ \Delta V_n \\ \Delta V_h \end{bmatrix}_i \tag{4}$$

where $\mathbf{c}^T$ denotes a coefficients vector of the controlled orbital elements emanating from the GVEs, as seen in Eqs. (2), and $\Delta\mathbf{v}$ is the concomitant impulsive velocity-correction vector.

C. Mean Orbital Elements Subject to a J_2 Perturbation

In the absence of perturbations, the six orbital elements remain constant. Because of the influence of J_2, some orbital elements will oscillate about a nominal value and others will exhibit secular drifts. The averaged values of the orbital elements are called the mean elements. If all the spacecraft in the formation are of equal type and build (i.e., have the same ballistic coefficient), then the differential J_2 acceleration is the dominant perturbation experienced by the spacecraft. In this case, the differential drag effect on the relative motion is negligible over a time period of several orbits.

The mean orbital elements under the effect of J_2 are determined by the differential equations [20]:

$$\frac{\mathrm{d}a}{\mathrm{d}t} = 0 \tag{5}$$

$$\frac{\mathrm{d}e}{\mathrm{d}t} = 0 \tag{6}$$

$$\frac{\mathrm{d}i}{\mathrm{d}t} = 0 \tag{7}$$

$$\frac{\mathrm{d}\Omega}{\mathrm{d}t} = -\frac{3}{2}J_2\left(\frac{R_e}{p}\right)^2 n\cos I \tag{8}$$

$$\frac{\mathrm{d}\omega}{\mathrm{d}t} = \frac{3}{4}J_2\left(\frac{R_e}{p}\right)^2 n(5\cos^2 I - 1) \tag{9}$$

$$\frac{\mathrm{d}M}{\mathrm{d}t} = n + \frac{3}{4}J_2\left(\frac{R_e}{p}\right)^2 n\sqrt{1-e^2}(3\cos^2 I - 1) \tag{10}$$

where R_e is the equatorial radius.

D. Mean Change of the Orbital Elements Because of Drag

If atmospheric rotation is neglected, then the inclination, the right ascension of the ascending node, and the argument of perigee are not affected by drag. The relationships for the averaged rates of the semimajor axis and the eccentricity, developed for a small eccentricity (expanding up to second-order in e), are given by [8]

$$\frac{\mathrm{d}a}{\mathrm{d}t} = -2\rho_p a^2 n K_D\left[\mathcal{I}_0 + 2e\mathcal{I}_1 + \frac{3e^2}{4}(\mathcal{I}_0 + \mathcal{I}_2)\right]\exp(-\beta a e) \tag{11}$$

$$\frac{\mathrm{d}e}{\mathrm{d}t} = -\rho_p K_D a n\left[2\mathcal{I}_1 + e(\mathcal{I}_0 + \mathcal{I}_2) - \frac{e^2}{4}(5I\mathcal{I}_1 + \mathcal{I}_3)\right]\exp(-\beta a e) \tag{12}$$

where $\mathcal{I}_k$ are modified Bessel functions of the first kind of order k and argument $\beta a e$, defined in the integral form,

$$\mathcal{I}_k(z) = \frac{1}{2\pi}\int_0^{2\pi} e^{z\cos\theta}\cos(k\theta)\,\mathrm{d}\theta \tag{13}$$

ρ_p is the atmospheric density at perigee, β is the inverse of the atmospheric scale height, and the ballistic coefficient is

$$K_D = \frac{sC_D}{2m}$$

where C_D is the drag coefficient, m is the spacecraft mass, and s is a reference area.

E. Relative Position and Velocity in Inertial Coordinates

To model the relative motion of the spacecraft under the preceding orbital perturbations, we will first write the inertial position and velocity of each spacecraft. This can be done by solving the Keplerian two-body problem in inertial coordinates and then extending the solution to include orbital perturbations using a standard variation-of-parameters procedure. The inertial position $\mathbf{r}$ and inertial velocity $\mathbf{v} = \dot{\mathbf{r}}$ are given by [20]

$$\mathbf{r} = \frac{a(1-e^2)}{1+e\cos f}\begin{bmatrix} \cos(f+\omega)\cos\Omega - \cos I\sin(f+\omega)\sin\Omega \\ \cos I\cos\Omega\sin(f+\omega) + \cos(f+\omega)\sin\Omega \\ \sin I\sin(f+\omega) \end{bmatrix} \tag{14}$$

$$\mathbf{v} = \dot{\mathbf{r}} = \sqrt{\frac{\mu}{a(1-e^2)}}[V_x, V_y, V_z]^T \tag{15}$$

where

$$V_x = -\cos\Omega\sin(f+\omega) - \sin\Omega\cos I\cos(f+\omega) - e(\cos\Omega\sin\omega + \sin\Omega\cos\omega\cos I)$$

$$V_y = \cos\Omega\cos I\cos(f+\omega) - \sin\Omega\sin(f+\omega) - e(\sin\Omega\sin\omega - \cos\Omega\cos\omega\cos I)$$

$$V_z = \sin I[\cos(f+\omega) + e\cos\omega]$$

In the presence of orbital perturbations and velocity corrections, the classical orbital elements vary with time. In this case, the inertial position and velocity are determined as follows:

1) Integrate the orbital elements with respect to time under orbital perturbations.

2) Calculate the inertial velocity until the moment of velocity correction.

3) Compute the inertial position by quadrature: $\mathbf{r} = \int \dot{\mathbf{r}}\,\mathrm{d}t$.

4) Perform an impulsive correction $\Delta\mathbf{v}$ (the required velocity-correction components are transformed from frame $\mathcal{T}$ to $\mathcal{I}$).

5) Determine the inertial velocity after the impulsive correction: $\mathbf{v}^+ = \mathbf{v}^- + \Delta\mathbf{v}$.

6) Integrate the orbital elements (step 1).

The relative velocity and relative position vectors in frame $\mathcal{I}$ between any two spacecraft S_j and S_i are defined as follows:

$$\dot{\mathbf{r}}_{i,j} = [Vx_{i,j}, Vy_{i,j}, Vz_{i,j}]^T = \dot{\mathbf{r}}_j - \dot{\mathbf{r}}_i \tag{16}$$

$$\mathbf{r}_{i,j} = [X_{i,j}, Y_{i,j}, Z_{i,j}]^T = \mathbf{r}_j - \mathbf{r}_i \tag{17}$$

III. Formation Topologies and Optimal Formationkeeping

In this section, we consider the relative motion of a group of N spacecraft S_i $(i = 1, \ldots, N)$. We will develop an impulsive-formationkeeping maneuver strategy for consuming minimum fuel.

The impulsive maneuver will be represented by a velocity-correction vector performed by each spacecraft, and the formation topology will be represented using elementary graph theory, briefly described in the following subsection.

A. Elementary Graph Theory

A graph is a pair $[G = (V, E)]$ of sets such that the elements of E are two-element subsets of V. The elements of V are the vertices or nodes, and the elements of E are the edges or arcs. The degree of a vertex v, $d_G(v)$, is the number of edges at v. A labeled graph is a graph with each node labeled differently (but arbitrarily), so that all nodes are considered to be distinct for the purpose of enumeration. A path $P = (V, E)$ on a labeled graph is a sequence

$$V = \{v_1, v_2, \ldots, v_N\}$$

such that

$$E = \{(v_1 v_2), (v_2 v_3), \ldots, (v_{N-1} v_N)\}$$

are the graph edges of the graph $G = (V, E)$. A closed path

$$P = v_1, v_2, \ldots, v_N, v_1$$

with $N \geq 3$ is called a graph cycle. The length of a cycle is its number of edges; a cycle of length m is denoted by C^m. A directed graph, or digraph, G is an ordered pair $[G = (V, A)]$, where V is a set of vertices or nodes and A is a set of ordered pairs of vertices (called directed edges, arcs, or arrows). An edge $e = (x, y)$ is considered to be directed from x to y (y is called the head and x is called the tail of the edge); y is said to be a direct successor of x, and x is said to be a direct predecessor of y. If a path leads from x to y, then y is said to be a successor of x, and x is said to be a predecessor of y. A tree T is a set of straight-line segments connected at their ends, containing no closed loops (cycles). In other words, it is a simple, undirected, connected, acyclic graph. A tree with N nodes has $N - 1$ graph edges. Conversely, a connected graph with N nodes and $N - 1$ edges is a tree. A labeled tree is a tree in which each vertex is given a unique label. The vertices of a labeled tree with n vertices are typically given the labels $1, 2, \ldots, n$. The leader graph is denoted by L^k; the leader graph is a tree, which is a directed graph. A spanning tree of a connected graph G is either the maximal set of edges of G that contains no cycles or the minimal set of edges that connect all vertices.

B. Relative-Orbital-Element Corrections

To develop an impulsive control for a group of N spacecraft, we shall treat this group as a digraph G^N and will term it the formation graph. Each spacecraft S_i $(i = 1, \ldots, N)$ constitutes a vertex in G^N. A relative-orbital-element correction of S_i and S_j, denoted by $\Delta\alpha_{i,j}$, constitutes an edge in G^N and is defined by

$$\Delta\alpha_{i,j} = \Delta\alpha_j - \Delta\alpha_i \tag{18}$$

where the orbital-element corrections of S_i and S_j in the presence of an impulsive velocity correction are, respectively,

$$\Delta\alpha_i = \alpha_i^+ - \alpha_i^- \tag{19}$$

$$\Delta\alpha_j = \alpha_j^+ - \alpha_j^- \tag{20}$$

where α^- is a value of the orbital element before an impulsive correction, and α^+ is the value of an orbital element after the impulsive correction. Therefore, a relative-orbital-element correction can be written as

$$\Delta\alpha_{i,j} = \Delta\alpha_j - \Delta\alpha_i = \alpha_j^+ - \alpha_j^- - (\alpha_i^+ - \alpha_i^-) \tag{21}$$

The relative-orbital-element corrections are indifferent to a particular predefined reference value chosen for an orbital element, α_{ref} (i.e., they are reference-orbit-independent); this can be seen by writing

$$\Delta\alpha_i = \alpha_i^+ - \alpha_{\text{ref}}, \qquad \Delta\alpha_j = \alpha_j^+ - \alpha_{\text{ref}} \tag{22}$$

and

$$\Delta\alpha_{i,j} = \Delta\alpha_j - \Delta\alpha_i = \alpha_j^+ - \alpha_i^+ \tag{23}$$

If the corrected orbital elements of S_i are to be equal to the orbital elements of S_j, then in the absence of perturbations, a formation will be created; this case is referred to as perturbation-free orbital-element matching. Semimajor axis (energy) matching in the case of Keplerian motion is a typical example [10]:

$$a_i^+ = a_j^+ \Rightarrow \Delta a_{i,j} = a_i^- - a_j^- \tag{24}$$

If perturbations are present, their effect will generally induce a relative drift. The basic requirement from the formation control law is to cancel the mean relative drift. When the relative deviation exceeds a maximum allowed value, a velocity correction should be applied. Each velocity correction sets the current value of the orbital-element correction to a new value that cancels future drifts. In this case, the corrected orbital elements of S_i and S_j satisfy the following condition:

$$\alpha_j^+ - \alpha_i^+ = \alpha_{i,j}^+ \tag{25}$$

and the relative element correction is

$$\Delta\alpha_{i,j} = \alpha_{i,j}^+ - \alpha_{i,j}^+ \tag{26}$$

where $\alpha_{i,j}^+$ is the required relative orbital element of S_i and S_j, defined as

$$\alpha_{i,j} = \alpha_j - \alpha_i$$

after the impulsive correction (this correction is determined based on the effect of drag and J_2, as will be shown in the sequel). Similarly, $\alpha_{i,j}^-$ is the relative orbital element before the impulsive correction.

C. Tree Topology

Let us assume for the moment that there are no perturbations present and that the formation is created by orbital-element matching. The spacecraft form a leader graph (i.e., a tree), as defined in Sec. III.A. Let us label the leader of this graph by S_1, with S_N being the root. Per this definition, the spacecraft form a leader formation L^N, and the resulting formation topology assumes the following form:

$$\begin{bmatrix} \Delta\alpha_{1,2} \\ \Delta\alpha_{2,3} \\ \vdots \\ \Delta\alpha_{N-1,N} \end{bmatrix} = \begin{bmatrix} 1 & -1 & 0 \cdots & 0 \\ 0 & 1 & -1 \cdots & 0 \\ \cdots & \cdots & \cdots & \cdots \\ 0 & 0 & 1 & -1 \end{bmatrix} \begin{bmatrix} \alpha_1^- \\ \alpha_2^- \\ \vdots \\ \alpha_N^- \end{bmatrix} \tag{27}$$

Using GVEs (2), we note that the orbital-element corrections can be expressed as a function of the velocity correction in the following manner:

$$\Delta\alpha_i = (\mathbf{c}_\alpha)_i^T \Delta\mathbf{v}_i, \qquad \Delta\alpha_j = (\mathbf{c}_\alpha)_j^T \Delta\mathbf{v}_j \tag{28}$$

where $(\mathbf{c}_\alpha)_i$ and $(\mathbf{c}_\alpha)_j$ are GVE coefficient vectors of S_i and S_j, respectively, as seen in Eqs. (2), and $\Delta\mathbf{v}_i$, $\Delta\mathbf{v}_j$ are the concomitant impulsive velocity-correction vectors. The relative-orbital-element correction can be thus written as follows:

$$\Delta\alpha_{i,j} = \Delta\alpha_j - \Delta\alpha_i = (\mathbf{c}_\alpha)_j^T \Delta\mathbf{v}_j - (\mathbf{c}_\alpha)_i^T \Delta\mathbf{v}_i \tag{29}$$

The state-space representation of this tree can be written as

$$A\boldsymbol{\Delta}\mathbf{v} = \mathbf{b} \tag{30}$$

where

$$A = \begin{bmatrix} -(\mathbf{c}_\alpha)_1^T & (\mathbf{c}_\alpha)_2^T & \mathbf{0}\cdots & \mathbf{0} \\ \mathbf{0} & -(\mathbf{c}_\alpha)_2^T & (\mathbf{c}_\alpha)_3^T\cdots & \mathbf{0} \\ \cdots & \cdots & \cdots & \cdots \\ \mathbf{0} & \mathbf{0}\cdots & -(\mathbf{c}_\alpha)_{N-1}^T & (\mathbf{c}_\alpha)_N^T \end{bmatrix} \tag{31}$$

is an $(N-1)\times 3N$ matrix, and

$$\mathbf{b} = \begin{bmatrix} \Delta\alpha_{1,2} \\ \Delta\alpha_{2,3} \\ \vdots \\ \Delta\alpha_{N-1,N} \end{bmatrix} \tag{32}$$

is a $(N-1)\times 1$ vector.

D. Balancing the Fuel Consumption

The use of relative-orbital-element corrections as edges in the tree topology has introduced an excess freedom into the formation graph; this can be plainly seen by the fact that the number of unknowns in Eq. (30) exceeds the number of constraints. This implies that a static parameter optimization problem with equality constrains can be solved; the only remaining issue is to choose the proper cost functional.

Choosing a cost functional that minimizes the total Δv of the formation seems to be the most straightforward selection [14–16]. For a formation of spacecraft equipped with separate impulsive thrusters for all three axes, this cost functional is [21]

$$\Delta v = \left\| \Delta\mathbf{v} \right\|_1 \triangleq \sum_{i=1}^{N} \left\| \Delta\mathbf{v}_i \right\|_1 \tag{33}$$

For spacecraft equipped with gimbaled thrusters, the minimum-fuel cost functional for the formation is

$$\Delta v = \left\| \Delta\mathbf{v} \right\|_2 \triangleq \sum_{i=1}^{N} \left\| \Delta\mathbf{v}_i \right\|_2 \tag{34}$$

In both cases, the cost functional constitutes the overall Δv of the formation. The rationale for choosing the overall Δv as the cost stems from the fact that the Δv is proportional to the amount of propellant Δm. This can be readily seen from the rocket equation:

$$\Delta m = m_0\left[1 - \exp\left(-\frac{\Delta v}{I_{\mathrm{sp}} g_0}\right)\right] \tag{35}$$

where m_0 is the initial fuel mass, I_{sp} is the specific impulse, and g_0 is the gravitational acceleration at sea level. For a first-order small Δm, Eq. (35) can be written as

$$\Delta v = \frac{\Delta m I_{\mathrm{sp}} g_0}{m_0} + \mathcal{O}(\Delta m^2) \tag{36}$$

However, minimizing either Eq. (33) or Eq. (34) may lead to a situation wherein some of the spacecraft consume much more propellant than the others. This unbalance can cause some of the spacecraft to run out of fuel faster than the others; if the formation is to be designed with identical or nearly identical spacecraft, each spacecraft must be designed for the worst-case fuel consumption, thus resulting in a conservative fuel budget for the entire formation.

To alleviate this situation, we propose using a penalty not on Δm, but rather on Δm^2. Although not necessarily minimizing the overall fuel consumption, this penalizes large individual fuel usage and balances the fuel among all the formation members. In this case, the spacecraft will tend to form a natural fuel-balanced formation: that is, to converge onto an orbit that does not require excessive fuel consumption from some of the formation members while preventing other spacecraft from maneuvering.

Penalizing Δm^2 implies penalizing Δv^2; again, this can be seen from Eq. (35):

$$\Delta v^2 = \frac{\Delta m^2 I_{\mathrm{sp}}^2 g_0^2}{m_0^2} + \mathcal{O}(\Delta m^3) \tag{37}$$

Thus, the problem of fuel-balanced optimal formationkeeping can be cast as follows. Find an optimal impulsive maneuver $\Delta\mathbf{v}^*$, satisfying

$$\Delta\mathbf{v}^* = \arg\min_{\Delta\mathbf{v}} \left\| \Delta\mathbf{v} \right\|_2^2 = \arg\min_{\Delta\mathbf{v}} \sum_{i=1}^{N} \left\| \Delta\mathbf{v}_i \right\|_2^2 \tag{38}$$

such that

$$A\Delta\mathbf{v} = \mathbf{b} \tag{39}$$

Augmenting the cost functional with the equality constrains using the Lagrange multiplier vector

$$\boldsymbol{\lambda} = [\lambda_1, \lambda_2, \ldots, \lambda_{N-1}]^T$$

yields

$$H = \|\Delta\mathbf{v}\|_2^2 + \boldsymbol{\lambda}^T(A\Delta\mathbf{v} - \mathbf{b}) \tag{40}$$

The necessary and sufficient conditions for the existence of minima are

$$\frac{\partial H}{\partial(\Delta\mathbf{v})} = \mathbf{0} \tag{41}$$

$$\frac{\partial^2 H}{\partial(\Delta\mathbf{v})^2} > 0 \tag{42}$$

The Hessian appearing in Eq. (42) is

$$\frac{\partial^2 H}{\partial(\Delta\mathbf{v})^2} = 2I_N \tag{43}$$

where I_N is an $N\times N$ identity matrix. Thus, the solution of Eq. (41) is always a minimum, meaning that the solution of the optimization problem (38) and (39) yields an optimal impulsive velocity-correction vector $\Delta\mathbf{v}^*$. This observation holds regardless of the particular spanning tree used to define the formation, as shown in Appendix A.

A straightforward approach for solving the optimization problem formulated in Eqs. (38) and (39) is to use the least-squares method. To that end, we rewrite expression (39) into

$$\begin{aligned}(A\Delta\mathbf{v} - \mathbf{b})(A\Delta\mathbf{v} - \mathbf{b})^T =& A\Delta\mathbf{v}(A\Delta\mathbf{v})^T - \mathbf{b}(A\Delta\mathbf{v})^T - A\Delta\mathbf{v}\mathbf{b}^T \\ &+ \mathbf{b}\mathbf{b}^T = A\Delta\mathbf{v}\Delta\mathbf{v}^T A^T - 2\mathbf{b}\Delta\mathbf{v}^T A^T + \mathbf{b}\mathbf{b}^T\end{aligned} \tag{44}$$

Taking the derivative with respect to $\Delta\mathbf{v}$ yields

$$2AA^T\Delta\mathbf{v} - 2A^T\mathbf{b} = 0 \tag{45}$$

Therefore, the minimizing vector $\Delta\mathbf{v}^*$ is a solution of the equation

$$AA^T\Delta\mathbf{v} = A^T\mathbf{b} \tag{46}$$

If the rows of A are linearly independent, then AA^T is invertible. In that case, the optimal solution of the system of linear equations is unique and is given by

$$\Delta\mathbf{v}^* = A^T(AA^T)^{-1}\mathbf{b} = A^+\mathbf{b} \tag{47}$$

where A^+ is the pseudoinverse of A.

IV. Control Strategy

The first goal of the control strategy is to initialize the spacecraft formation and then to keep the spacecraft in the leader graph L^N even in the presence of perturbations. In the absence of perturbations, the necessary and sufficient condition guaranteeing a stable formation is that the mean motions of S_i and S_j form a 1:1 resonant motion. Because the periods of Keplerian elliptic orbits are determined by the

orbital energy, this requirement can be transformed into an energy matching condition [10] or, equivalently, semimajor-axis matching.

However, orbital perturbations induce temporal changes in the orbital elements of each spacecraft. In general, the effects of perturbations on each spacecraft are not the same. The Earth oblateness effect is a function of the semimajor axis, eccentricity, and inclination. Because of initialization errors, small initial differences of the semimajor axis, eccentricity, and inclination lead to secular changes in both the nodal rate $\dot{\Omega}$ and the mean latitude rate $\dot{M}+\dot{\omega}$. These differences lead to a buildup of out-of-plane and in-plane angular separations. In addition, not all the spacecraft involved in the formation are of equal type, mass, shape, and attitude profile. These physical variations lead to drag differences that cause secular changes in the semimajor axis and the eccentricity, which in turn lead to secular changes in the nodal rate and the mean latitude rate due to the Earth oblateness.

The formationkeeping control law is required to mitigate the relative deviations of the mean drift of $\dot{\Omega}$ and $\dot{M}+\dot{\omega}$. That could be done by persistently matching semimajor axis, eccentricity, and inclination.

A. Optimal Corrections of the Semimajor Axis, Eccentricity, and Inclination

Two different scenarios should be considered. The first is when all the spacecraft in the formation experience the same drag; the relative drift of the orbital elements is then zero. The second scenario is when the effect of natural perturbations on each spacecraft is different.

To preserve the formation, a periodic velocity correction should be applied. As already discussed, the corrected elements a_i^+, e_i^+, and I_i^+ $(i=1,\ldots,N)$ would theoretically remain unchanged in the absence of drag perturbations, and no further correction of these elements would be needed. However, when a drag difference exists, the elements a_i^+, e_i^+, and I_i^+ $(i=1,\ldots,N)$ slowly deviate from the initial values until an additional velocity correction must be applied. The time interval between subsequent corrections is chosen according to the allowed deviation. When the deviation exceeds the allowed maximum, a new velocity correction is performed. Each velocity correction sets the element to cancel future drifts due to drag.

Choosing to control semimajor axis, eccentricity, and inclination leads to a relationship in the form of Eq. (30). Let us define the matrices A_a, A_e, and A_I representing the mapping of the velocity corrections to the relative-orbital-element corrections $\Delta a_{i,j}$, $\Delta e_{i,j}$, and $\Delta I_{i,j}$ $(i=1,\ldots,N)$ based on GVEs (2):

$$A_a=\begin{bmatrix} -(c_a)_1 & (c_a)_2 & 0\cdots & \mathbf{0}_{(1\times N)} & \mathbf{0}_{(1\times N)} \\ 0 & -(c_a)_2 & (c_a)_3\cdots & \mathbf{0}_{(1\times N)} & \mathbf{0}_{(1\times N)} \\ \vdots & \ddots & \vdots & \ddots & \vdots \\ 0\cdots & -(c_a)_{N-1} & (c_a)_N & \mathbf{0}_{(1\times N)} & \mathbf{0}_{(1\times N)} \end{bmatrix} \tag{48}$$

where $(c_a)_i$ is given by [compare with Eqs. (2)]

$$(c_a)_i=\frac{2v_i a_i^2}{\mu} \tag{49}$$

Similarly,

$$A_e=\begin{bmatrix} -(c_e)_1 & (c_e)_2 & 0\cdots & -(s_e)_1 & (s_e)_2 & 0\cdots & \mathbf{0}_{(1\times N)} \\ 0 & -(c_e)_2 & (c_e)_3\cdots & 0 & -(s_e)_1 & (s_e)_3\cdots & \mathbf{0}_{(1\times N)} \\ \vdots & \ddots & \ddots & \ddots & \ddots & \vdots & \vdots \end{bmatrix} \tag{50}$$

where

$$(c_e)_i=\frac{2(e_i+\cos f_i)}{v_i},\qquad (s_e)_i=-\frac{r_i\sin f_i}{v_i a_i} \tag{51}$$

and

$$A_i=\begin{bmatrix} \mathbf{0}_{(1\times N)} & \mathbf{0}_{(1\times N)} & -(k_I)_1 & (k_I)_2 & 0\cdots \\ \mathbf{0}_{(1\times N)} & \mathbf{0}_{(1\times N)} & 0 & -(k_I)_2 & (k_I)_3\cdots \\ \vdots & \ddots & \ddots & \ddots & \vdots \end{bmatrix} \tag{52}$$

where

$$(k_I)_i=\frac{r_i\cos(f_i+\omega_i)}{h_i} \tag{53}$$

Finally, in the absence of perturbations, Eq. (30) assumes the following form:

$$\begin{bmatrix} A_a \\ A_e \\ A_I \end{bmatrix}\begin{bmatrix} (\Delta V_t)_1 \\ (\Delta V_t)_2 \\ \vdots \\ (\Delta V_t)_N \\ (\Delta V_n)_1 \\ (\Delta V_n)_2 \\ \vdots \\ (\Delta V_n)_N \\ (\Delta V_h)_1 \\ (\Delta V_h)_2 \\ \vdots \\ (\Delta V_h)_N \end{bmatrix}=\begin{bmatrix} \Delta a_{1,2} \\ \Delta a_{2,3} \\ \vdots \\ \Delta a_{N,N-1} \\ \Delta e_{1,2} \\ \Delta e_{2,3} \\ \vdots \\ \Delta e_{N,N-1} \\ \Delta I_{1,2} \\ \Delta I_{2,3} \\ \vdots \\ \Delta I_{N,N-1} \end{bmatrix} \tag{54}$$

which complies with the general form of Eq. (39).

When perturbations are present, the vector $\mathbf{b}$ becomes a superposition of the precorrected relative orbital elements and the final relative orbital elements, as shown in Eq. (26). Thus, the formationkeeping topology developed here is generic; the only difference between the perturbed and unperturbed cases is the entries of $\mathbf{b}$.

B. Closed-Form Expressions for Optimal Impulsive Formationkeeping

Consider the following scenario: A formation graph G^3 is located in nearby orbits with different initial semimajor-axis values. In the absence of perturbations, this graph will form a stable formation if the energies of S_1, S_2, and S_3 are equal or, equivalently, if the semimajor axes of their orbits are identical. We will show that the preceding optimal formationkeeping scheme can yield analytic closed-form expressions for the optimal impulsive maneuvers required to match the semimajor axes using the least-squares method.

The initial values of semimajor axes and velocities of G^3 are a_1, a_2, and a_3 and v_1, v_2, and v_3, respectively, and the relative semimajor axes corrections are

$$\Delta a_{2,1}=\Delta a_2-\Delta a_1 \tag{55}$$

$$\Delta a_{3,2}=\Delta a_3-\Delta a_2 \tag{56}$$

The matrix A_a, which is given by Eqs. (48) and (49), assumes the following form:

$$A_a=\begin{bmatrix} -\frac{2v_1a_1^2}{\mu} & \frac{2v_2a_2^2}{\mu} & 0 \\ 0 & -\frac{2v_2a_2^2}{\mu} & \frac{2v_3a_3^2}{\mu} \end{bmatrix} \tag{57}$$

The optimal impulsive maneuver is calculated using the least-squares method:

$$\Delta\mathbf{v}^*=A_a^T(A_aA_a^T)^{-1}\mathbf{b},\qquad \mathbf{b}=[\Delta a_{2,1},\Delta a_{3,2}]^T \tag{58}$$

The optimal velocity corrections required to match the semimajor axes of the spacecraft are given by

$$(\Delta V_t^\star)_1 = -\frac{1}{2}\frac{\mu v_1 a_1^2\left(v_2^2 a_2^4 \Delta a_{3,2} + v_2^2 a_2^4 \Delta a_{2,1} + v_3^2 a_3^4 \Delta a_{2,1}\right)}{v_1^2 a_1^4 v_3^2 a_3^4 + v_1^2 a_1^4 v_2^2 a_2^4 + v_3^2 a_3^4 v_2^2 a_2^4} \tag{59}$$

$$(\Delta V_t^\star)_2 = \frac{1}{2}\frac{\mu v_2 a_2^2\left(v_3^2 a_3^4 \Delta a_{2,1} - v_1^2 a_1^4 \Delta a_{3,2}\right)}{v_1^2 a_1^4 v_3^2 a_3^4 + v_1^2 a_1^4 v_2^2 a_2^4 + v_3^2 a_3^4 v_2^2 a_2^4} \tag{60}$$

$$(\Delta V_t^\star)_3 = \frac{1}{2}\frac{\mu v_3 a_3^2\left(v_1^2 a_1^4 \Delta a_{3,2} + v_2^2 a_2^4 \Delta a_{3,2} + v_2^2 a_2^4 \Delta a_{2,1}\right)}{v_1^2 a_1^4 v_3^2 a_3^4 + v_1^2 a_1^4 v_2^2 a_2^4 + v_3^2 a_3^4 v_2^2 a_2^4} \tag{61}$$

and the resulting semimajor-axis corrections are

$$\Delta a_i^\star = \frac{2a_i^2 v_i}{\mu}(\Delta V_t^\star)_i \tag{62}$$

yielding

$$\Delta a_1^\star = -\frac{v_1^2 a_1^4\left(v_2^2 a_2^4 \Delta a_{3,2} + v_2^2 a_2^4 \Delta a_{2,1} + v_3^2 a_3^4 \Delta a_{2,1}\right)}{v_1^2 a_1^4 v_3^2 a_3^4 + v_1^2 a_1^4 v_2^2 a_2^4 + v_3^2 a_3^4 v_2^2 a_2^4} \tag{63}$$

$$\Delta a_2^\star = -\frac{a_2^4 v_2^2\left(v_3^2 a_3^4 \Delta a_{2,1} - v_1^2 a_1^4 \Delta a_{3,2}\right)}{v_1^2 a_1^4 v_3^2 a_3^4 + v_1^2 a_1^4 v_2^2 a_2^4 + v_3^2 a_3^4 v_2^2 a_2^4} \tag{64}$$

$$\Delta a_3^\star = \frac{a_3^4 v_3^2\left(v_1^2 a_1^4 \Delta a_{3,2} + v_2^2 a_2^4 \Delta a_{3,2} + v_2^2 a_2^4 \Delta a_{2,1}\right)}{v_1^2 a_1^4 v_3^2 a_3^4 + v_1^2 a_1^4 v_2^2 a_2^4 + v_3^2 a_3^4 v_2^2 a_2^4} \tag{65}$$

All the spacecraft in G^3 will match their semimajor axes to some value $a^\star$. The value of $a^\star$ corresponds to the balanced velocity correction required to form a formation in the absence of perturbations and is given by

$$a^\star = a_i + \Delta a_i^\star \tag{66}$$

It can be shown that $a^\star$ is the centroid of the initial values of the semimajor axis:

$$a^\star = \frac{1}{N}\sum_{i=0}^{N} a_i \tag{67}$$

This value of $a^\star$ yields the globally optimal total velocity correction in the sense of minimizing $\|\Delta\mathbf{v}\|_2^2$ for all possible values of a reference semimajor axis (this result is valid only for controlling each orbital element separately).

V. Optimal Formationkeeping Under Perturbations: Identical Ballistic Coefficients

In this section, we will implement the new control strategy on a formation of J_2-perturbed spacecraft having identical ballistic coefficients. We will extend the method to the general case in the next section. To illustrate the main idea, consider a formation of four spacecraft flying in a low Earth orbit. All spacecraft have the same ballistic coefficient and a small initial difference in the values of the semimajor axis and eccentricity. In this case, as was described in Sec. IV, to form a stable formation, one can match semimajor axis and eccentricity, then the relative deviations of the mean drifts $\dot{\Omega}$ and $\dot{M} + \dot{\omega}$ would be zero. The initial orbital elements and ballistic coefficients are summarized in Table 1.

Table 1 Initial orbital elements and ballistic coefficients of a formation in a low Earth orbit.

S_i	a, km	e	I, rad	Ω, rad	ω, rad	f_0, rad	K_D
S_1	6928.2	0.0012	0.01	0	0	0	0.0355
S_2	6928.3	0.0013	0.01	0	0	0	0.0355
S_3	6928.5	0.0014	0.01	0	0	0	0.0355
S_4	6928.8	0.0015	0.01	0	0	0	0.0355

The initial differences in semimajor axis and eccentricity lead to a buildup of angular separation between the orbital planes of the spacecraft, $\Omega_{i,j}$, and of the in-plane angular separation $(M+\omega)_{i,j}$, which increases the distance between spacecraft, $d_{i,j}$. We shall now demonstrate the implementation of the proposed formationkeeping method (matching semimajor axis, eccentricity, and inclination).

Figures 1 and 2 depict the time history of the mean relative orbital elements. The impulsive maneuver is applied at $f = 90$ deg after 1.25 orbits. It can be seen that relative drift of the mean relative orbital elements is stopped. Although the values of semimajor axis and eccentricity decrease due to drag, the formation remains intact, and the distances between spacecraft are bounded. Figure 3 shows the time history of the relative velocity components $Vx_{i,j}$, $Vy_{i,j}$, and $Vz_{i,j}$ in inertial coordinates [Eq. (16)]. The discontinuity in the relative velocity components is a result of the impulsive velocity correction. Following the impulsive maneuver, the position components exhibit a bounded periodic motion. This can be seen in Fig. 4, showing the three-dimensional relative orbit in inertial coordinates and the projections thereof on the X–Y, X–Z, and Y–Z planes.

VI. Optimal Formationkeeping of Spacecraft with Different Ballistic Coefficients

In this section, we study the motion of a formation of spacecraft having different ballistic coefficients, and we develop an optimal formationkeeping algorithm based on the least-squares formalism developed in Sec. III. Different ballistic coefficients cause different secular changes of semimajor axis and eccentricity for each spacecraft, which in turn lead to different secular changes of the nodal rate and the mean latitude rate, due to the Earth oblateness. Periodic velocity corrections must then be applied, because the corrected orbital elements will continue to deviate from the reference values.

To that end, we will implement the optimal impulsive scheme developed herein while relying on an auxiliary dynamic equations developed by Mishne [8]. The auxiliary relations will be used to calculate the required corrections of the semimajor axis and the eccentricity that will cancel relative drifts in the nodal angle and the mean latitude angle until the next velocity correction. We shall also suggest a new method for mitigating the cross-coupling of the orbital-element corrections (semimajor axis and eccentricity are corrected by applying tangential and normal maneuvers; this correction affects the mean latitude rate as well).

Before commencing with our development of the formationkeeping strategy, we will highlight some important differences between the current work and the method of Mishne [8]:

1) We propose controlling nodal rate and mean latitude rate *indirectly*, by selecting suitable values of semimajor axis and eccentricity. These values are chosen to cancel future drifts until the next velocity correction. It is possible to choose which two of the three elements to control because there are only two constraints: namely, equalizing the out-of-plane and in-plane drifts.

2) Fuel optimization is done according to the method described in Sec. III. Controlling semimajor axis and eccentricity leads to in-plane velocity corrections only. By finding a suitable timing for these corrections, it is possible to minimize the effect of changes in ω and M due to the impulsive corrections in the tangential and normal directions.

3) We offer an optimal solution by not imposing a global reference orbit a priori.

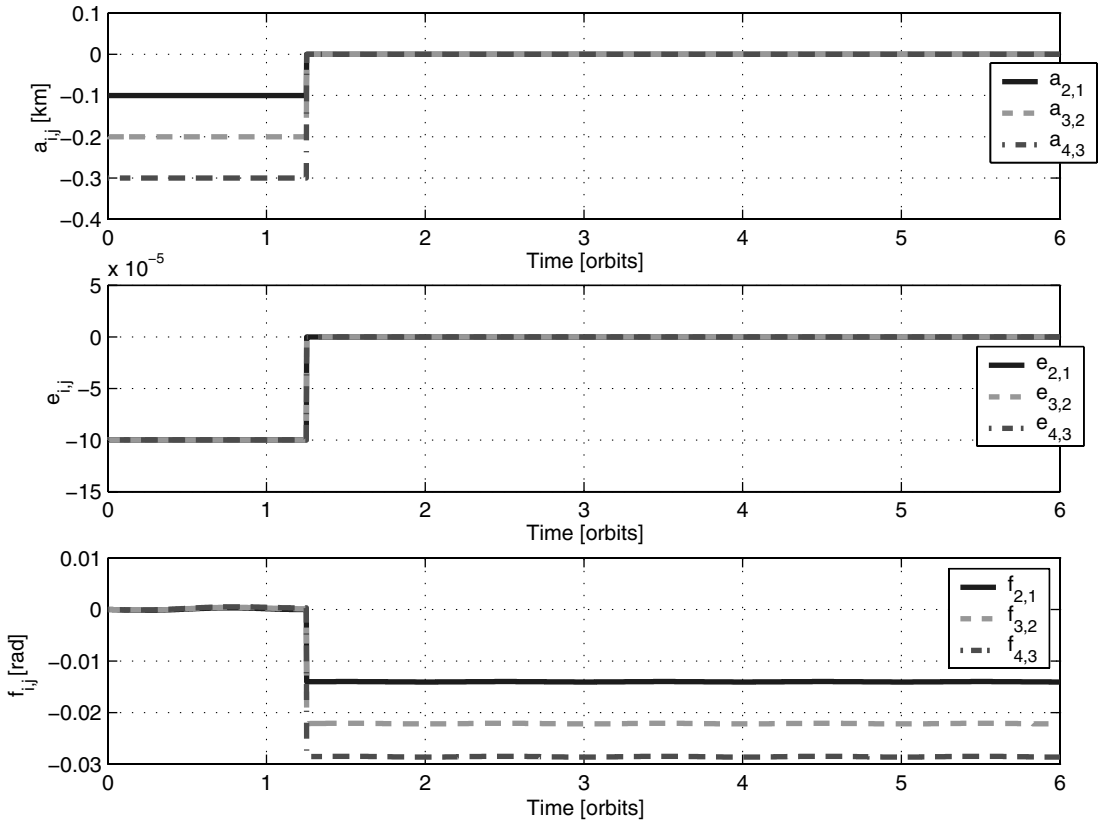

Fig. 1 Mean values of the relative semimajor axis and eccentricity and the true anomaly, with an optimal velocity correction applied.

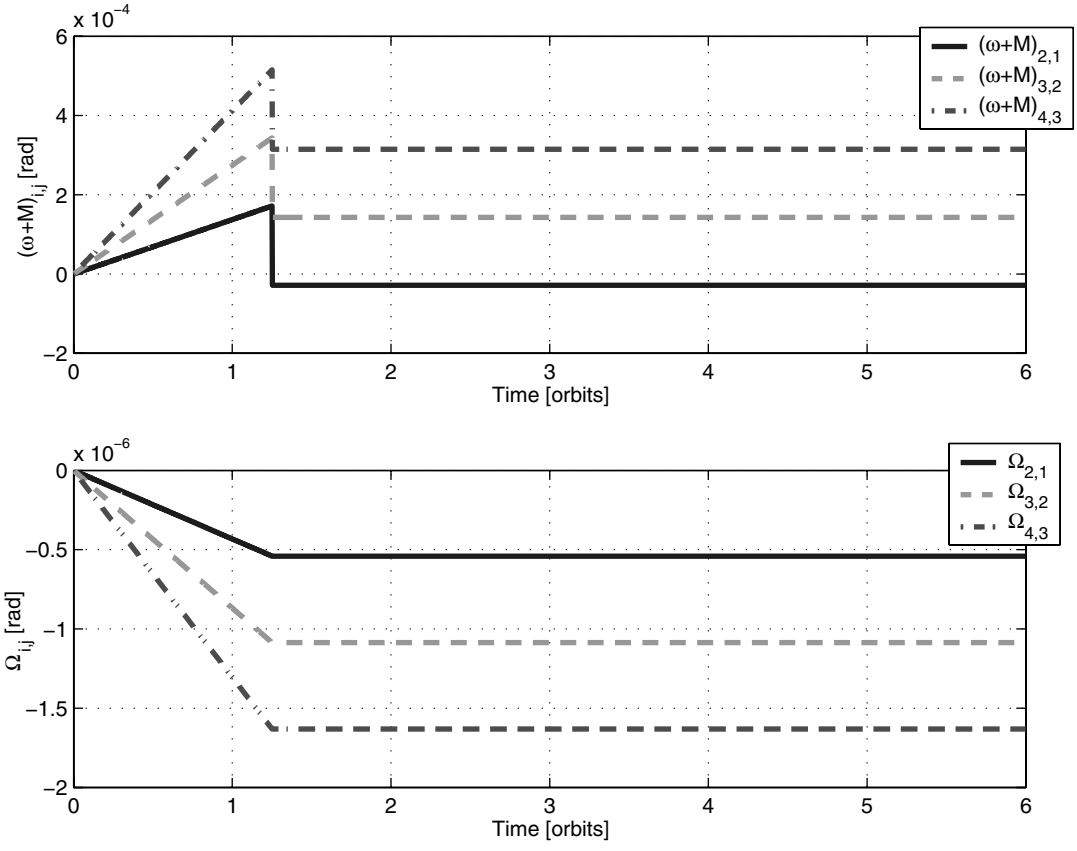

Fig. 2 Relative drift in $\omega + M$ and Ω is arrested after a velocity correction.

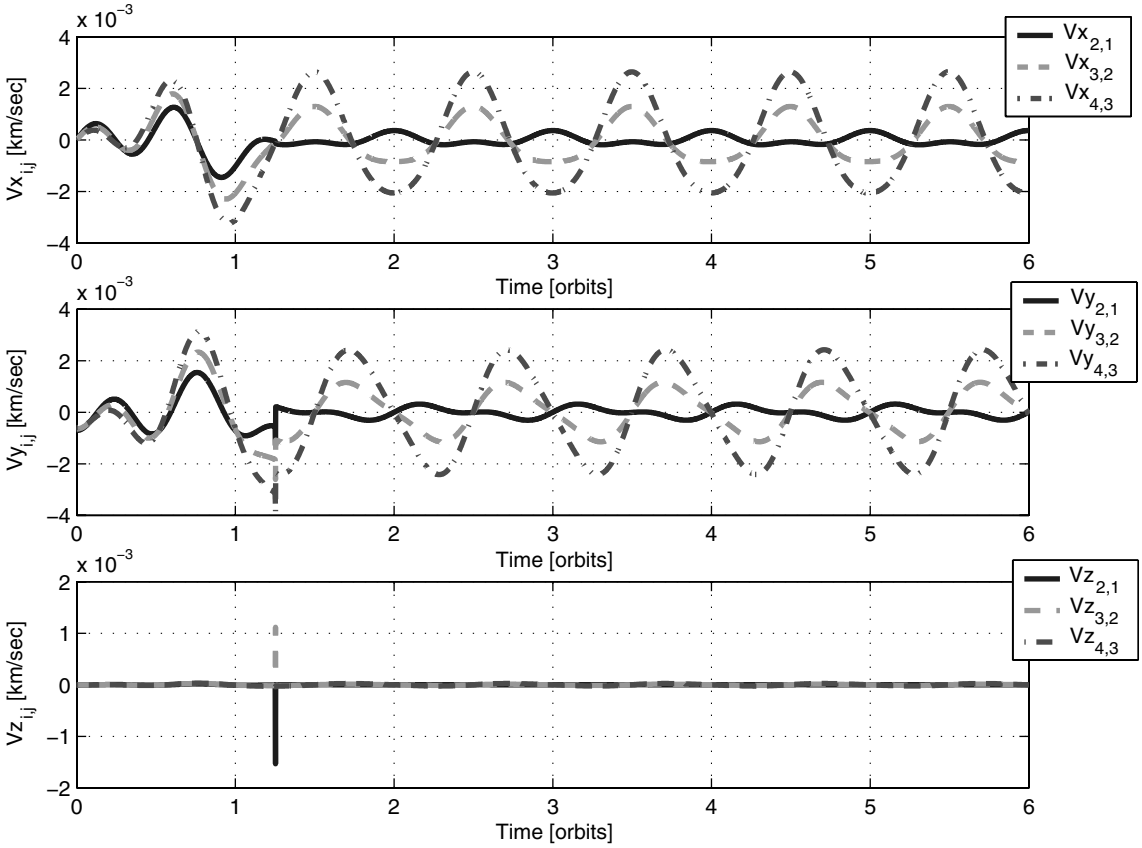

Fig. 3 Relative velocity components in the inertial frame, with an impulsive correction, become bounded.

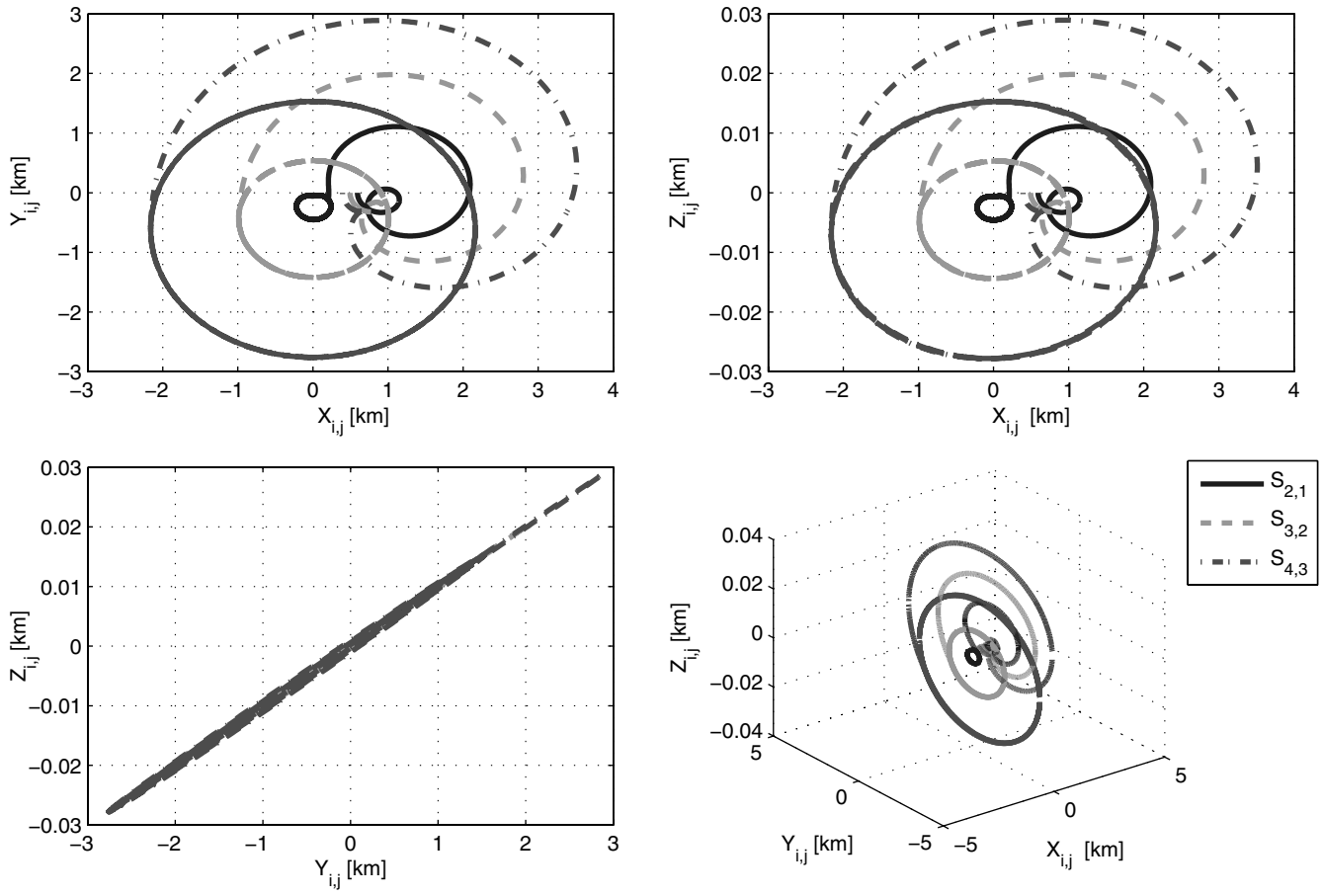

Fig. 4 Relative motion in inertial coordinates exhibits bounded orbits following the formationkeeping maneuver, performed after 1.25 orbits.

A. Calculation of the Required Correction of Semimajor Axis and Eccentricity

In the presence of J_2 and drag, the relative orbital elements of any S_i are determined by the GVEs given in Sec. II. The perturbed dynamics of these elements can be written in the general form:

$$\dot{\boldsymbol{\alpha}} = \mathbf{F}(\boldsymbol{\alpha}) \tag{68}$$

where $\mathbf{F} = [F_1, \ldots, F_6]^T$ is a vector-valued function $\mathbf{F}$: $\mathbb{R}^6 \to \mathbb{R}^6$. If the initial orbital elements of S_i are different from those of S_j, and in addition there exists a difference ΔK_D in the ballistic coefficients, then linearizing Eq. (68) about $\boldsymbol{\alpha}_i$ entails [8]

$$\dot{\boldsymbol{\alpha}}_{i,j} \approx Q\boldsymbol{\alpha}_{i,j} + \mathbf{q}\Delta K_D \tag{69}$$

where

$$Q = \{Q_{lm}\} = [\partial \mathbf{F}/\partial \boldsymbol{\alpha}]_{\boldsymbol{\alpha}=\boldsymbol{\alpha}_i} \in \mathbb{R}^{6\times 6}$$

and

$$\mathbf{q} = [q_1, \ldots, q_6]^T = [\partial \mathbf{F}/\partial K_D]_{\boldsymbol{\alpha}=\boldsymbol{\alpha}_i} \in \mathbb{R}^6$$

The entries of Q and $\mathbf{q}$ pertinent for the subsequent calculations are given by [8]

$$Q_{41} = \frac{\partial F_4}{\partial a} = \frac{21}{4} J_2 \left(\frac{R_e}{p}\right)^2 \frac{n}{a} \cos I \tag{70}$$

$$Q_{42} = \frac{\partial F_4}{\partial e} = -6J_2 R_e^2 \frac{nae}{p^3} \cos I \tag{71}$$

$$Q_{51} = \frac{\partial F_5}{\partial a} = -Q_{41} \frac{5\cos^2 I - 1}{2\cos I} \tag{72}$$

$$Q_{52} = \frac{\partial F_5}{\partial e} = -Q_{42} \frac{5\cos^2 I - 1}{2\cos I} \tag{73}$$

$$Q_{61} = \frac{\partial F_6}{\partial a} = \frac{3n}{2a}\left[1 + \frac{7}{4} J_2 \sqrt{1-e^2}\left(\frac{R_e}{p}\right)^2 (3\cos^2 I - 1)\right] \tag{74}$$

$$Q_{62} = \frac{\partial F_6}{\partial e} = \frac{9}{4} J_2 n \left(\frac{R_e}{p}\right)^2 (3\cos^2 I - 1) \frac{e}{(1-e^2)^{\frac{5}{2}}} \tag{75}$$

and

$$q_4 = \frac{\partial F_4}{\partial K_D} = 0, \qquad q_5 = \frac{\partial F_5}{\partial K_D} = 0, \qquad q_6 = \frac{\partial F_6}{\partial K_D} = 0 \tag{76}$$

To control the orbital-element deviations, impulsive velocity corrections must be applied. An impulsive velocity correction causes an instantaneous change of the orbital elements $\Delta\boldsymbol{\alpha}_d$. The relationship between the velocity change and the element change is given by GVEs (3). The velocity correction is chosen to satisfy [8]:

$$\dot{\Omega}_{i,j} = \dot{\Omega}^+_{i,j}, \qquad (\dot{M} + \dot{\omega})_{i,j} = (\dot{M} + \dot{\omega})^+_{i,j} \tag{77}$$

When a drag difference exists, $\boldsymbol{\alpha}^+_{i,j}$ constitutes an initial condition, and the deviation changes according to Eq. (69). Thus, the desired drift rates are set to values that will compensate for the effect of drag differences until next correction.

By combining Eqs. (3) and (69) the following two conditions for the desired correction values of semimajor axis and eccentricity are obtained [8]:

$$\mathbf{L}_1 \boldsymbol{\alpha}^+_{i,j} + q_4 \Delta K_D = \dot{\Omega}^+_{i,j} \tag{78}$$

$$\mathbf{L}_2 \boldsymbol{\alpha}^+_{i,j} + (q_5 + q_6)\Delta K_D = (\dot{M} + \dot{\omega})^+_{i,j} \tag{79}$$

where the vector $\mathbf{L}_1$ is the fourth row of Q, $\mathbf{L}_2$ is the sum of the fifth and sixth rows of Q, and q_i are the elements of $\mathbf{q}$. This procedure results in

$$Q_{41} a^+_{i,j} + Q_{42} e^+_{i,j} + Q_{43} I^+_{i,j} = \dot{\Omega}^+_{i,j} \tag{80}$$

$$(Q_{51} + S_{61}) a^+_{i,j} + (Q_{52} + Q_{62}) e^+_{i,j} + (Q_{53} + Q_{63}) I^+_{i,j} = (\dot{M} + \dot{\omega})^+_{i,j} \tag{81}$$

Equations (81) are two linear equations for the three desired relative orbital elements $(a^+_{i,j}, e^+_{i,j}, I^+_{i,j})$. This means that there is a single degree-of-freedom. Because $a^+_{i,j}$ and $e^+_{i,j}$ depend upon the ballistic coefficient and $I^+_{i,j}$ is unaffected by either J_2 or by ΔK_D, we will assume that $I^+_{i,j} = 0$. This yields two linear equations with two unknowns, $a^+_{i,j}$ and $e^+_{i,j}$, for which the solution is

$$e^+_{i,j} = \frac{(\dot{M} + \dot{\omega})^+_{i,j} - (Q_{51} + Q_{61})\dot{\Omega}^+_{i,j}/Q_{41}}{(Q_{52} + Q_{62}) - Q_{42}/Q_{41}(Q_{51} + Q_{61})} \tag{82a}$$

$$a^+_{i,j} = \frac{\Omega^+_{i,j} - Q_{42} e^+_{i,j}}{Q_{41}} \tag{82b}$$

Finally, the optimal velocity correction $\Delta\mathbf{v}^*$ is calculated using Eq. (47) and is given by [compare with Eq. (54)]:

$$\Delta\mathbf{v}^* = \begin{bmatrix} A_a \\ A_e \end{bmatrix}^+ \begin{bmatrix} a^-_{1,2} + a^+_{1,2} \\ a^-_{2,3} + a^+_{2,3} \\ \vdots \\ a^-_{N,N-1} + a^+_{2,3} \\ e^-_{1,2} + e^+_{1,2} \\ e^-_{2,3} + e^+_{1,2} \\ \vdots \\ e^-_{N,N-1} + e^+_{N,N-1} \end{bmatrix} = \begin{bmatrix} A_a \\ A_e \end{bmatrix}^+ \begin{bmatrix} \Delta a_{1,2} \\ \Delta a_{2,3} \\ \vdots \\ \Delta a_{N,N-1} \\ \Delta e_{1,2} \\ \Delta e_{2,3} \\ \vdots \\ \Delta e_{N,N-1} \end{bmatrix} = \begin{bmatrix} A_a \\ A_e \end{bmatrix}^+ \mathbf{b} \tag{83}$$

where A_a and A_e are matrices defined in Eqs. (48–51), and the vector $\mathbf{b}$ is a superposition of the precorrected relative orbital elements and the desired corrections in semimajor axis and eccentricity given by Eq. (82).

B. Calculation of the Desired Drifts

The desired drifts immediately following the velocity correction, $\dot{\Omega}^+_{i,j}$ and $(\dot{M} + \dot{\omega})^+_{i,j}$, are chosen to be in the opposite direction of the expected drift due to drag that will be accumulated until the next correction. These values will be used in Eq. (82). The velocity correction will yield initial drift rates that are opposite to the drift due to drag. These drifts can be found using a linear approximation, valid for a short time interval T between two subsequent corrections [8]:

$$\dot{\Omega}^+_{i,j} = -\frac{1}{2}(Q_{41}F_1 + Q_{42}F_2)\frac{\Delta K_D}{K_D} T \tag{84}$$

$$(\dot{M} + \dot{\omega})^+_{i,j} = -\frac{1}{2}[(Q_{51} + Q_{61})F_1 + (Q_{52} + Q_{62})F_2]\frac{\Delta K_D}{K_D} T \tag{85}$$

Table 2 Initial orbital elements of four spacecraft with different ballistic coefficients

S_i	a, km	e	I, rad	Ω, rad	ω, rad	f_0, rad	K_D
S_1	6803	0.0012	0.01	0	0	0	0.0355
S_2	6803	0.0012	0.01	0	0	0	0.03905
S_3	6803	0.0012	0.01	0	0	0	0.036
S_4	6803	0.0012	0.01	0	0	0	0.0396

C. Minimization of the Cross-Coupling Effect

A well-known difficulty in controlling spacecraft orbits using impulsive velocity corrections is the cross-coupling between orbital elements. In formation-flying problems, this effect renders finding conditions for bounded relative motion quite difficult.

Semimajor axis and eccentricity are corrected by applying in-plane velocity corrections ΔV_t and ΔV_n. These velocity corrections in turn cause undesirable changes in M and ω, creating an in-plane separation $(M+\omega)_{i,j}$ each time the velocity correction is performed. However, the orbital elements depend upon true anomaly. This fact can be used to mitigate the coupling of orbital-element corrections. For example, a tangential velocity correction applied at periapsis or apoapsis will not cause any change in ω, and a normal velocity correction applied at $f = 90$ or 270 deg will not influence M.

We will now derive a method for mitigating the in-plane cross-coupling. This can be done if the semimajor axis and eccentricity corrections are performed twice per orbit. The first correction is performed at $f = 90$ deg and the second is performed at $f = 270$ deg. Let us denote the correction of an orbital element α at these points by $\Delta\alpha^{\mathrm{I}}$ and $\Delta\alpha^{\mathrm{II}}$, respectively.

Because the change in semimajor axis and eccentricity due to drag is slow, we can adopt the following approximation:

$$\Delta a^{\mathrm{I}} \approx \Delta a^{\mathrm{II}} \tag{86}$$

$$\Delta e^{\mathrm{I}} \approx \Delta e^{\mathrm{II}} \tag{87}$$

This gives

$$\Delta a^{\mathrm{I}} = \frac{2(a^{\mathrm{I}})^2 v^{\mathrm{I}}}{\mu}\Delta V_t^{\mathrm{I}} = \frac{2(a^{\mathrm{II}})^2 v^{\mathrm{II}}}{\mu}\Delta V_t^{\mathrm{II}} = \Delta a^{\mathrm{II}} \tag{88}$$

From which it immediately follows that $\Delta V_t^{\mathrm{I}} = \Delta V_t^{\mathrm{II}}$ (under the assumption that $v^{\mathrm{I}} \approx v^{\mathrm{II}} = v$ and $a^{\mathrm{I}} \approx a^{\mathrm{II}} = a$). Similarly,

$$\Delta e^{\mathrm{I}} = \frac{2e^{\mathrm{I}}}{v^{\mathrm{I}}}\Delta V_t^{\mathrm{I}} - \frac{r^{\mathrm{I}}}{a^{\mathrm{I}}}\Delta V_n^{\mathrm{I}} = \frac{2e^{\mathrm{II}}}{v^{\mathrm{II}}}\Delta V_t^{\mathrm{II}} + \frac{r^{\mathrm{II}}}{a^{\mathrm{II}}}\Delta V_n^{\mathrm{II}} = \Delta e^{\mathrm{II}} \tag{89}$$

yielding $\Delta V_n^{\mathrm{I}} = -\Delta V_n^{\mathrm{II}}$ (assuming that $e^{\mathrm{I}} \approx e^{\mathrm{II}} = e$ and $r^{\mathrm{I}} \approx r^{\mathrm{II}} = r$).

The parasitic change in ω and in M due to the first velocity correction is given by

$$\Delta\omega^{\mathrm{I}} = \frac{2}{ev}\Delta V_{t^{\mathrm{I}}} + 2e\Delta V_n^{\mathrm{I}} \tag{90a}$$

$$\Delta M^{\mathrm{I}} = -\frac{b}{eav}\left[2\left(1+\frac{e^2 r}{p}\right)\Delta V_t^{\mathrm{I}}\right] \tag{90b}$$

and the unwanted change in ω and in M due to second velocity correction is given by

$$\Delta\omega^{\mathrm{II}} = -\frac{2}{ev}\Delta V_t^{\mathrm{II}} + 2e\Delta V_n^{\mathrm{II}} \tag{91a}$$

$$\Delta M^{\mathrm{II}} = \frac{b}{eav}\left[2\left(1+\frac{e^2 r}{p}\right)\Delta V_t^{\mathrm{II}}\right] \tag{91b}$$

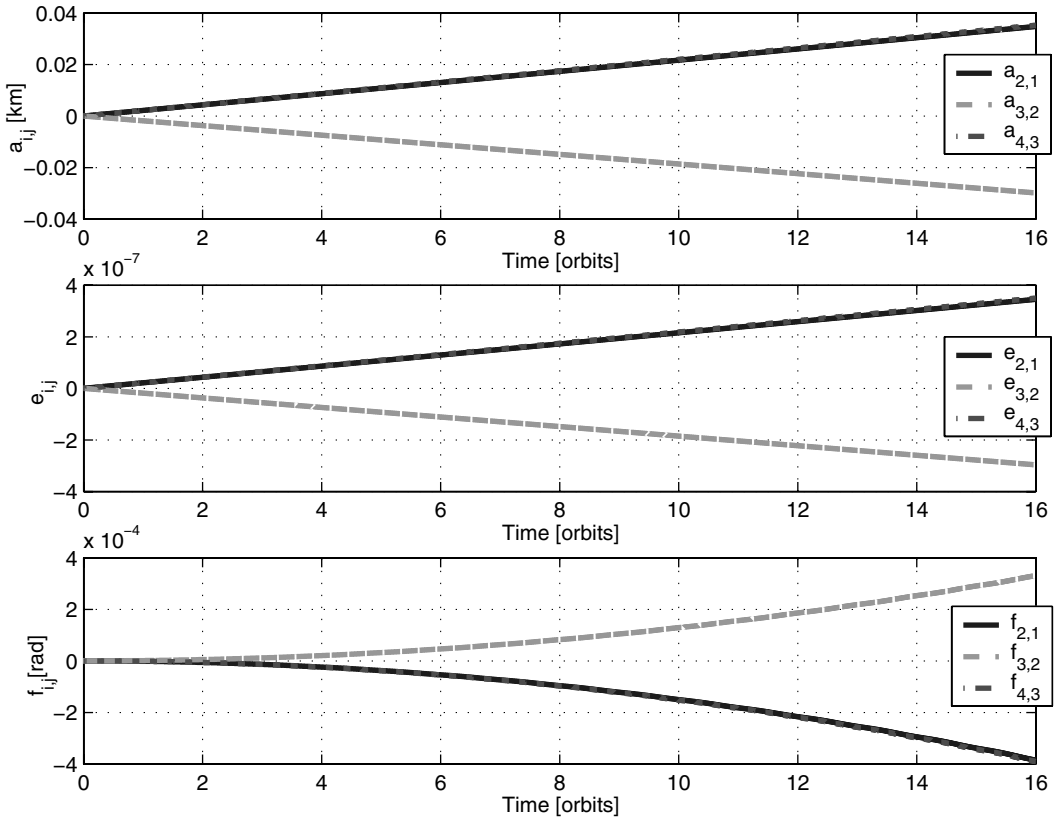

Fig. 5 Growth of the mean relative semimajor axis, eccentricity and true anomaly due to different ballistic coefficients, without applying formationkeeping maneuvers.

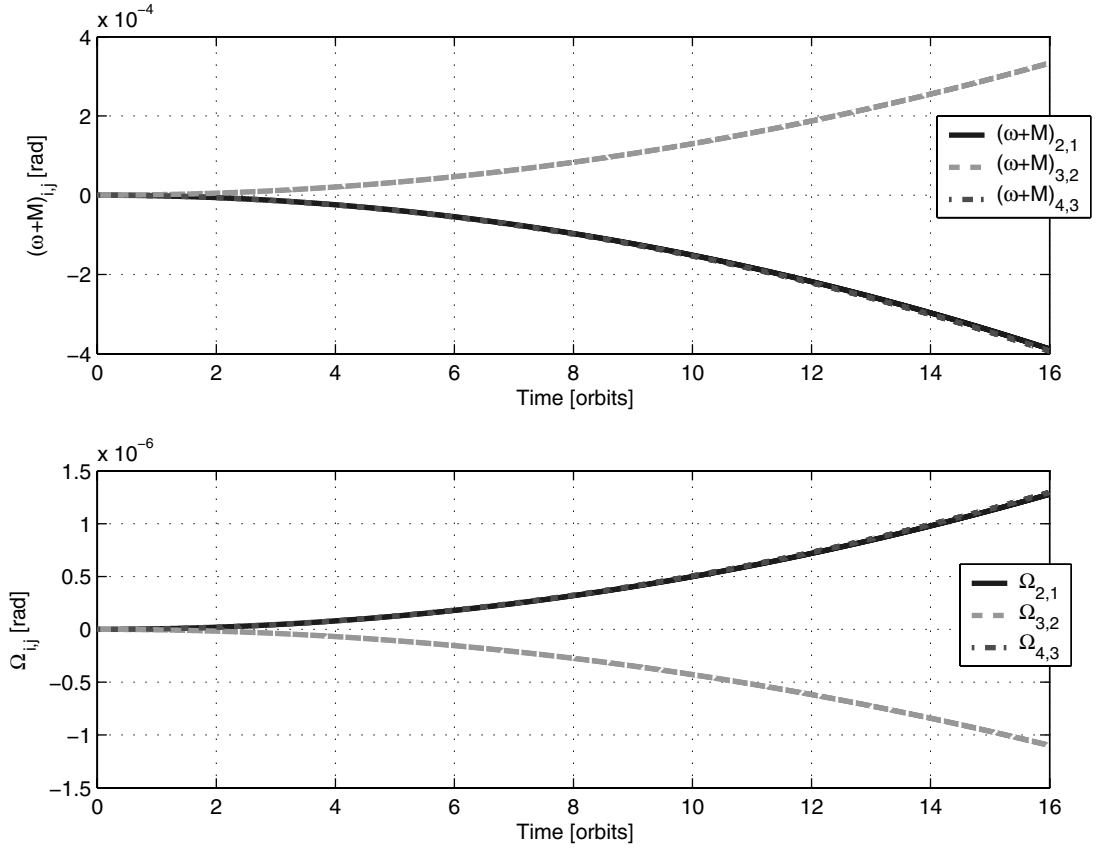

Fig. 6 In-plane and out-of-plane angular separation due to different ballistic coefficients, without applying a formationkeeping maneuver.

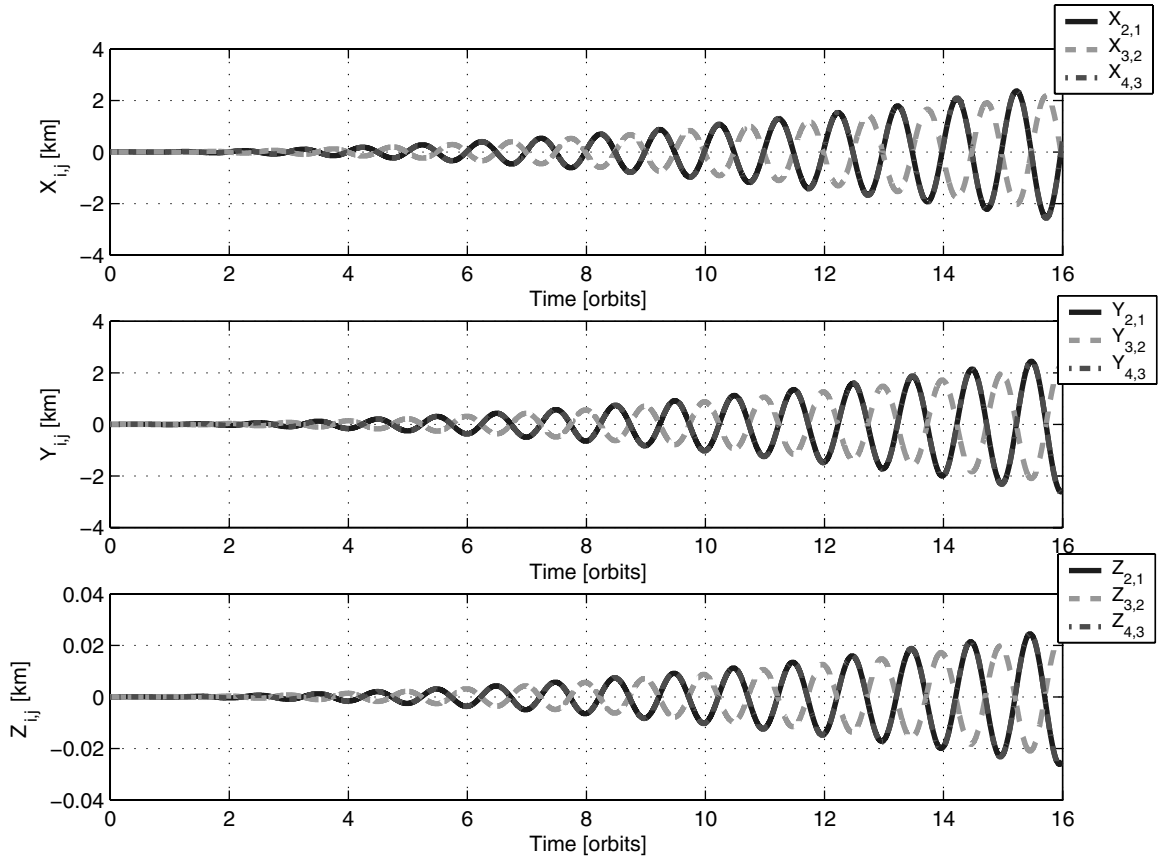

Fig. 7 Relative drift of the relative position components due to different ballistic coefficients, without applying a velocity correction.

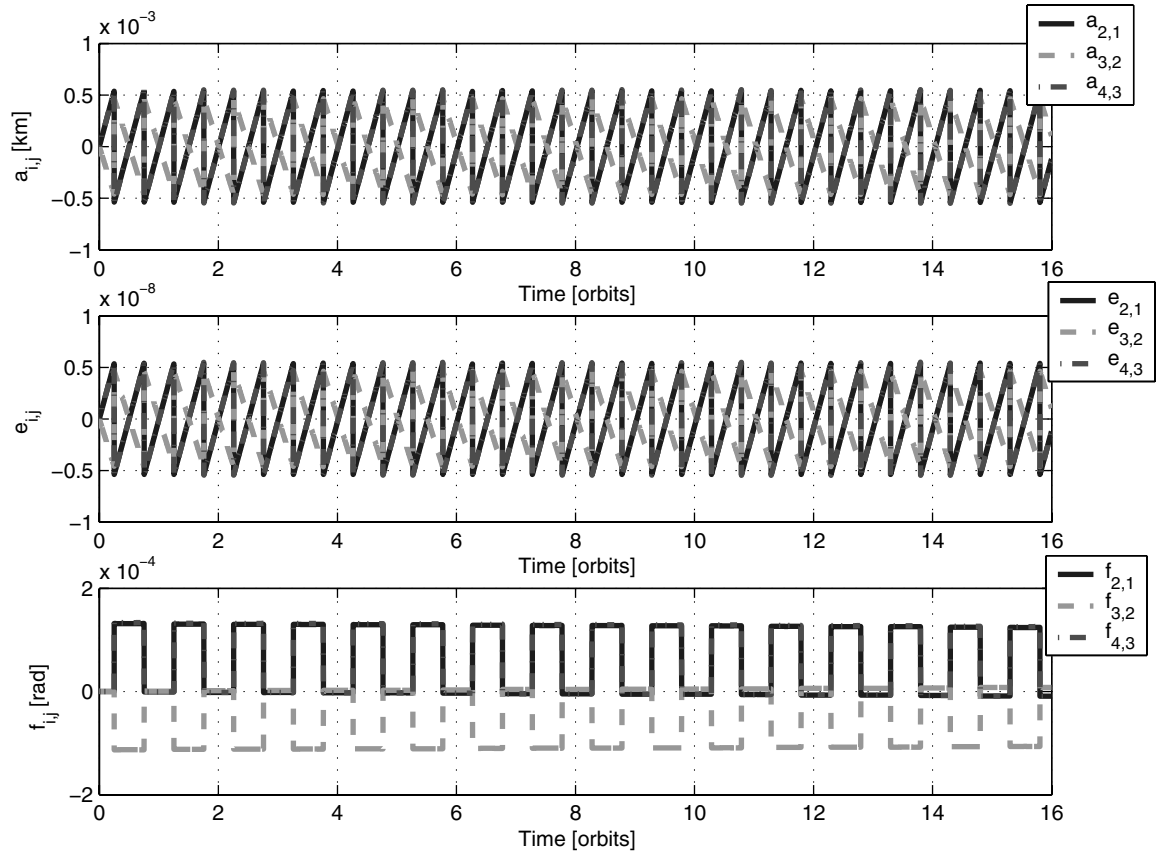

Fig. 8 Time history of the mean relative values of the semimajor axis and eccentricity, and the true anomaly with different ballistic coefficients, using optimal velocity corrections.

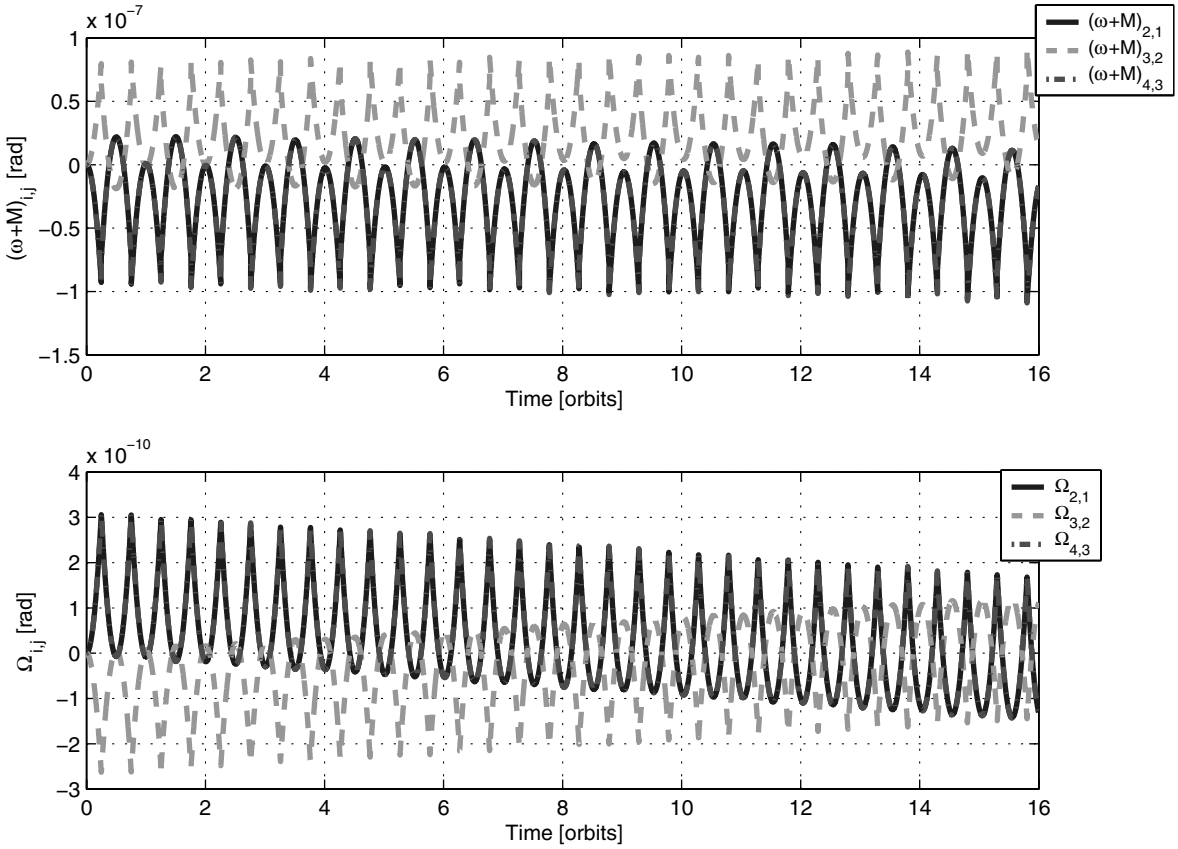

Fig. 9 Time history of the in-plane and out-of-plane angular separation with different ballistic coefficients using periodic velocity corrections. The angular drifts are minuscule.

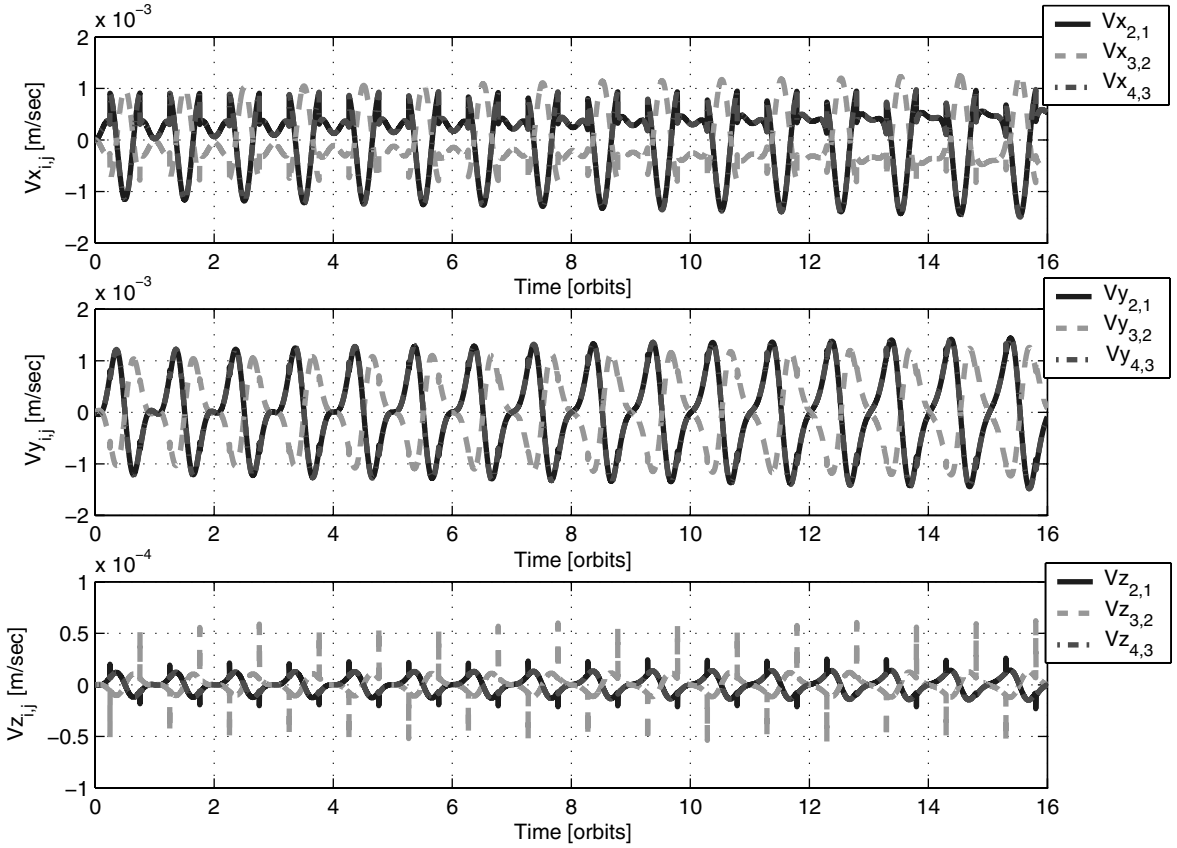

Fig. 10 Relative velocity components with different ballistic coefficients and periodic velocity corrections.

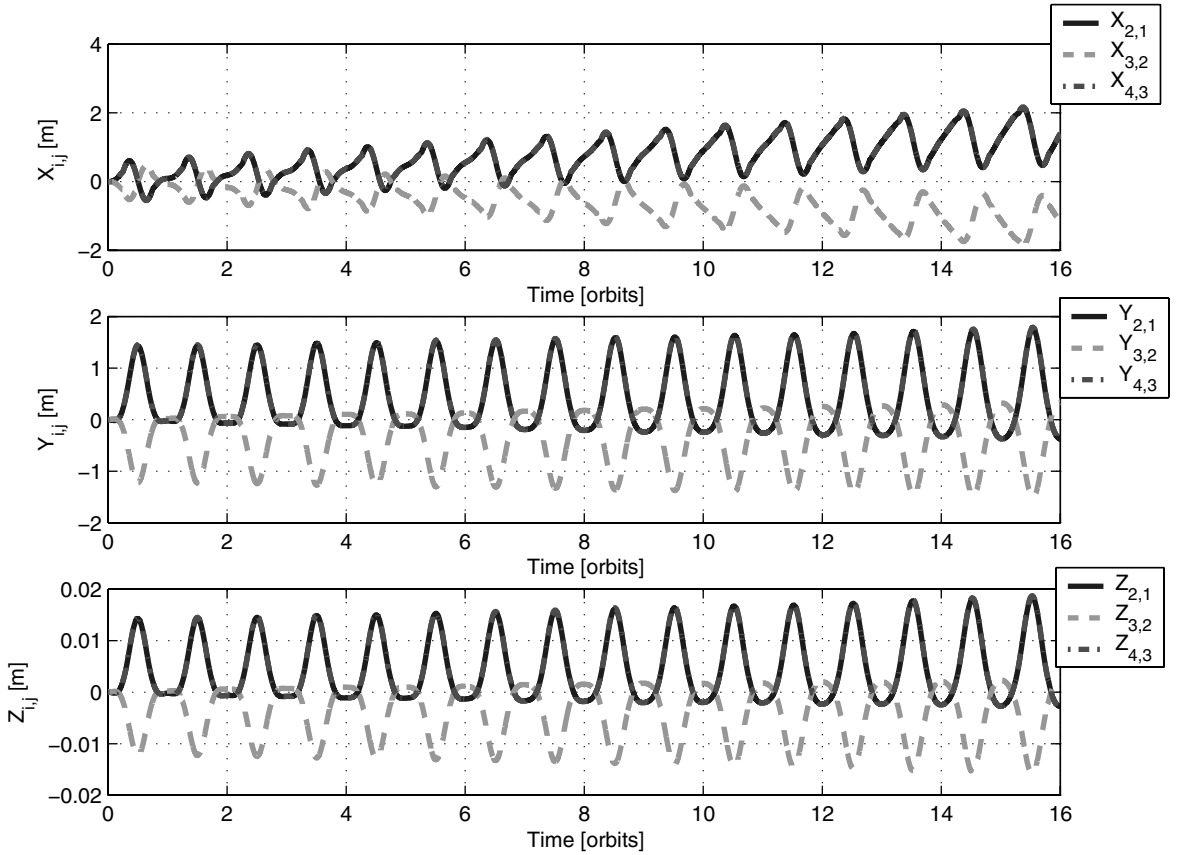

Fig. 11 The position components in inertial coordinates with different ballistic coefficients under periodic velocity corrections, optimally calculated to mitigate the effect of differential perturbations.

By combining Eqs. (90) with Eqs. (91), we get the total in-plane deviation during an orbital period:

$$(\Delta\omega^{\mathrm{I}} + \Delta\omega^{\mathrm{II}}) + (\Delta M^{\mathrm{I}} + \Delta M^{\mathrm{II}}) = 0 \tag{92}$$

which means that if we perform in-plane corrections at these points, a second in-plane change will cancel out the first parasitic in-plane change.

D. Simulation

First, we will simulate the uncontrolled motion of the spacecraft in a 425-km low Earth orbit. The differences in ballistic coefficients between the spacecraft are about 10%. The initial orbital elements and ballistic coefficients are summarized in Table 2. As can be seen in Figs. 5 and 6, different ballistic coefficients cause different drifts in semimajor axis and eccentricity, which in turn induces secular differences in the out-of-plane and in-plane angular motions due to the J_2 effect. Figure 7 depicts the relative position components in inertial coordinates. The difference in ballistic coefficients increases the relative position components so that the average distance between the formation-flying spacecraft amount to about 2.5 km after 16 orbits.

Next, we demonstrate that the proposed formationkeeping method [Eq. (83)] considerably reduces the relative drift. The orbital elements are corrected twice per orbit, at $f = 90$ and 270 deg, thus minimizing the effect of cross-coupling between the orbital elements. As shown in Figs. 8 and 9, the periodic impulsive corrections almost nullify the relative drift in the relative orbital elements. Figures 10 and 11 show the time history of the relative velocity and position components, respectively, in inertial coordinates. The discontinuities in the relative velocity components are a result of the impulsive velocity corrections that are performed twice per orbit. Figure 12 shows the three-dimensional relative orbits and the projections of the relative orbits onto the X–Y, X–Z, and Y–Z planes in inertial coordinates. Figure 13 depicts the distance between spacecraft. The drift is not zero, but it is much smaller than the uncorrected case (about three orders of magnitude, relative to the uncorrected case). A small in-plane drift remains because the cross-coupling effect causes a small residual drift in relative position. The actual in-plane drift is not identically zero because of the assumption we made that the change in semimajor axis and eccentricity due to drag is slow. The maximum separation is between S_4 and S_3 and is about 2.5 m after 16 orbits (one day).

E. Fuel Consumption

The fuel required for formationkeeping is related to the total velocity change by the rocket equation (35). The total velocity change can be calculated by either Eq. (33) or Eq. (34), depending on the type of propulsion system. For a mission lifetime of five years, the total velocity corrections of each spacecraft, calculated according to Eq. (34), are

$$\begin{aligned} \Delta v_{\mathrm{tot}_1} &= 19.89 \text{ m/s}, & \Delta v_{\mathrm{tot}_2} &= 14.78 \text{ m/s} \\ \Delta v_{\mathrm{tot}_3} &= 14.97 \text{ m/s}, & \Delta v_{\mathrm{tot}_4} &= 20.26 \text{ m/s} \end{aligned} \tag{93}$$

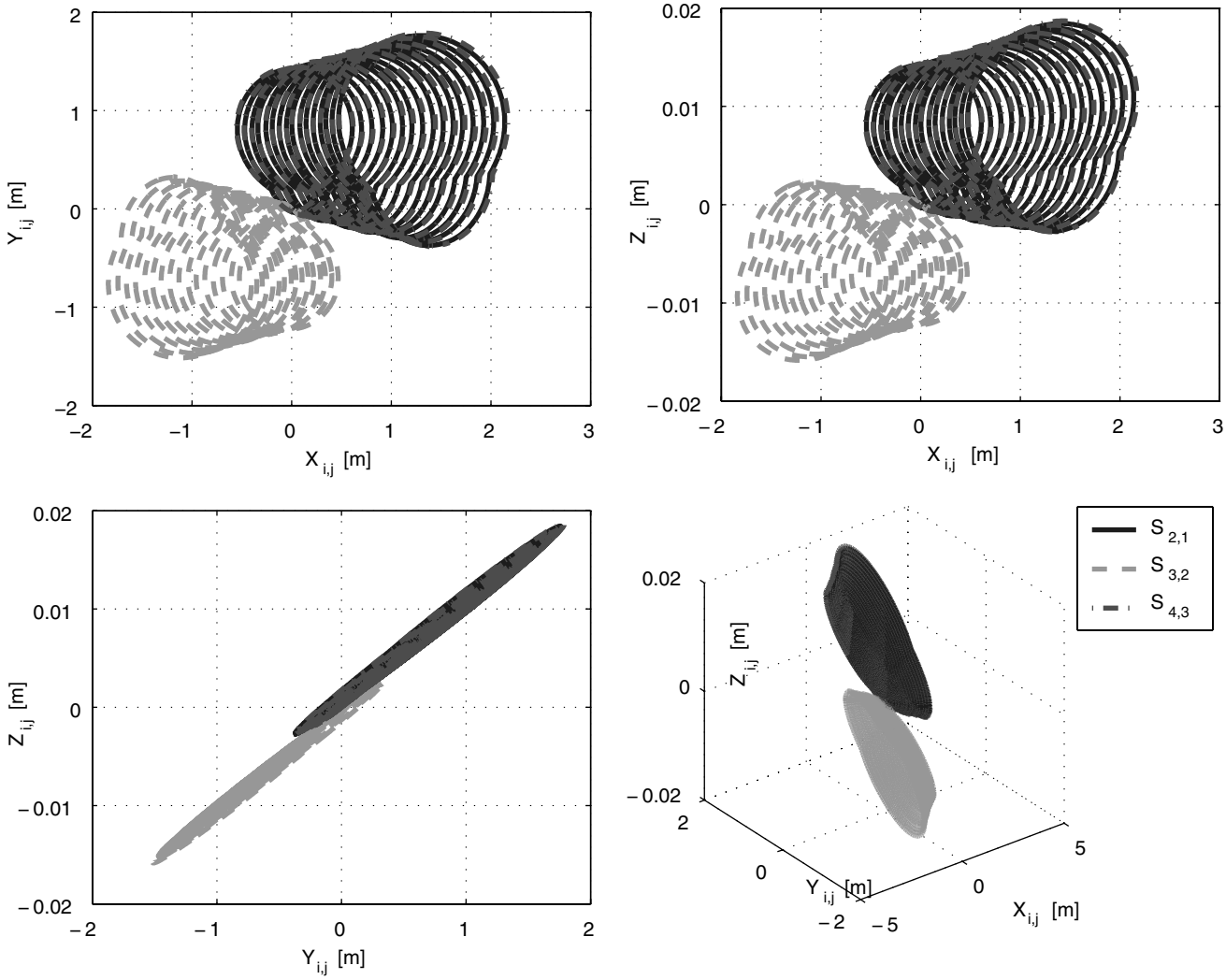

Fig. 12 Relative motion between spacecraft with different ballistic coefficients in inertial coordinates, using periodic velocity corrections. The drift is reduced by three orders of magnitude compared with the uncontrolled case.

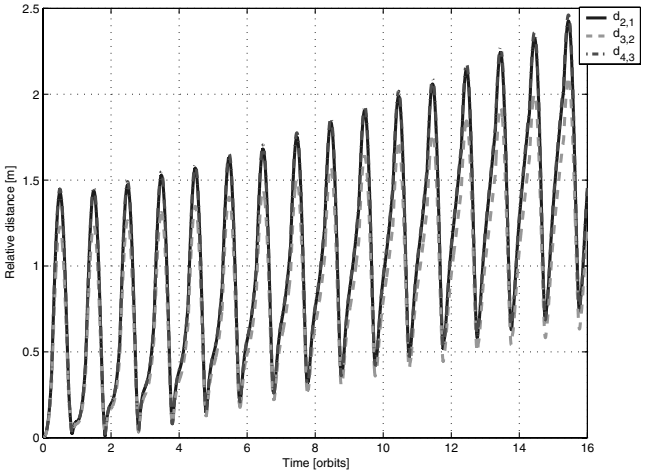

Fig. 13 Relative distance between spacecraft with different ballistic coefficients shows that a maximum separation of only 2.5 m after 16 orbits.

and the total Δv is about 70 m/s. The actual propellent consumption can be calculated according to the rocket equation (35). Taking $I_{sp} = 220$ s and $m_0 = 500$ kg, the required fuel mass for each spacecraft is as follows:

$$\Delta m_1 = 4.59 \text{ kg}, \qquad \Delta m_2 = 3.41 \text{ kg}$$
$$\Delta m_3 = 3.46 \text{ kg}, \qquad \Delta m_4 = 4.67 \text{ kg} \tag{94}$$

We thus see that the propellent mass is properly balanced among the formation spacecraft. For comparison, the total five-year velocity corrections calculated according to Eq. (33) are

$$\Delta v_{\text{tot}_1} = 23.12 \text{ m/s}, \qquad \Delta v_{\text{tot}_2} = 17.16 \text{ m/s}$$
$$\Delta v_{\text{tot}_3} = 17.45 \text{ m/s}, \qquad \Delta v_{\text{tot}_4} = 23.41 \text{ m/s} \tag{95}$$

and the total velocity correction is about 81 m/s.

VII. Conclusions

We developed a generic fuel-balanced impulsive maneuver scheme for multiple spacecraft formationkeeping using relative-orbital-element corrections. The spacecraft formation was modeled as a directed graph, an approach that accommodates any number of spacecraft. More important, formulating the problem of formationkeeping in terms of relative-orbital-element corrections left the final values of the controlled elements unconstrained. This freedom was used to find optimal impulsive maneuvers, in the sense of minimizing the l^2-norm, for formation initialization and control in the presence of perturbations.

The main conclusions are as follows:

1) A controlled group of spacecraft will form a pattern in the position space that corresponds to the optimal velocity correction.

2) Leaving the reference orbit free results in a globally optimal velocity correction.

3) This velocity correction can be analytically computed using a simple least-squares procedure.

Because the formationkeeping formalism is formulated in terms of relative-orbital-element corrections, one can choose which orbital elements to control. The final differences in the controlled elements can be constrained to minimize the effect of orbital perturbations and cross-coupling.

The newly developed algorithm was illustrated by a simulation of a formation of four spacecraft flying in low Earth orbits subject to J_2 and drag perturbations. Two different scenarios were examined. The first is when all spacecraft possess identical ballistic coefficients, and the second is when the spacecraft have different ballistic coefficients.

In the first scenario, the most dominant perturbation is J_2. Because of initialization errors, small initial differences of the semimajor axis, eccentricity, and inclination lead to secular changes in both the nodal rate and the mean latitude rate. The formationkeeping algorithm is then required to cancel theses relative mean drifts. This was achieved by matching semimajor axis, eccentricity, and inclination.

In the second scenario, a periodic velocity correction should be applied to preserve the formation, because the corrected orbital elements deviate from the reference values due to different ballistic coefficients. We proposed controlling the nodal rate and the mean latitude rate indirectly, by selecting suitable values of semimajor axis and eccentricity. These values were selected to cancel future drifts until the next velocity correction. The simulation results showed that applying the newly developed formationkeeping reduced the relative drift by three orders of magnitude.

Appendix A: Effect of Different Spanning Trees on the Velocity-Correction Vector

According to Cayley's formula, the number of different spanning trees of the connected graph G^N is N^{N-2}, where each spanning tree forms a different labeled graph [22]. In the previous sections, we treated the spacecraft formation as a leader formation L^N, which is also a labeled graph. The leader of this formation was labeled S_1. This means that for a formation of N spacecraft, we can form N^{N-2} different A matrices and $\mathbf{b}$ vectors. The analysis in this paper was performed for a formation represented by the particular spanning tree

$$S_N \to S_{N-1} \to \cdots \to S_1$$

We will now examine how different spanning trees affect the velocity correction required from each spacecraft and the total velocity correction. For simplicity, we will study only semimajor-axis corrections. To that end, consider all 16 possible spanning trees for a formation of four spacecraft, as shown in Fig. A1. We arbitrarily choose four different spanning trees: L_1^4, L_7^4, L_{13}^4, and L_{16}^4. These trees are shown in Fig. A1. The initial values of semimajor axes for this formation are as follows:

$$a_1 = 42,160 \text{ km}, \qquad a_2 = 42,167 \text{ km},$$
$$a_3 = 42,170 \text{ km}, \qquad a_4 = 42,185 \text{ km} \tag{A1}$$

The matrices Aa_1, Aa_7, Aa_{13}, and Aa_{16} and the vectors $\mathbf{b}_1$, $\mathbf{b}_7$, $\mathbf{b}_{13}$, and $\mathbf{b}_{16}$, corresponding to the trees L_1^4, L_7^4, L_{13}^4, and L_{16}^4 are as follows:

$$(A_a)_1 = \begin{bmatrix} \frac{-2v_1a_1^2}{\mu} & \frac{2v_2a_2^2}{\mu} & 0 & 0 \\ 0 & \frac{-2v_2a_2^2}{\mu} & \frac{2v_3a_3^2}{\mu} & 0 \\ 0 & 0 & \frac{-2v_3a_3^2}{\mu} & \frac{2v_4a_4^2}{\mu} \end{bmatrix}, \qquad \mathbf{b}_1 = \begin{bmatrix} \Delta a_{2,1} \\ \Delta a_{3,2} \\ \Delta a_{4,3} \end{bmatrix} \tag{A2}$$

$$(A_a)_7 = \begin{bmatrix} \frac{-2v_1a_1^2}{\mu} & \frac{2v_2a_2^2}{\mu} & 0 & 0 \\ \frac{-2v_1a_1^2}{\mu} & 0 & \frac{2v_3a_3^2}{\mu} & 0 \\ 0 & 0 & \frac{-2v_3a_3^2}{\mu} & \frac{2v_4a_4^2}{\mu} \end{bmatrix}, \qquad \mathbf{b}_7 = \begin{bmatrix} \Delta a_{2,1} \\ \Delta a_{3,1} \\ \Delta a_{4,3} \end{bmatrix} \tag{A3}$$

$$(A_a)_{13} = \begin{bmatrix} \frac{-2v_1a_1^2}{\mu} & \frac{2v_2a_2^2}{\mu} & 0 & 0 \\ 0 & \frac{-2v_2a_2^2}{\mu} & \frac{2v_3a_3^2}{\mu} & 0 \\ 0 & \frac{-2v_2a_2^2}{\mu} & 0 & \frac{2v_4a_4^2}{\mu} \end{bmatrix}, \qquad \mathbf{b}_{13} = \begin{bmatrix} \Delta a_{2,1} \\ \Delta a_{3,2} \\ \Delta a_{4,2} \end{bmatrix} \tag{A4}$$

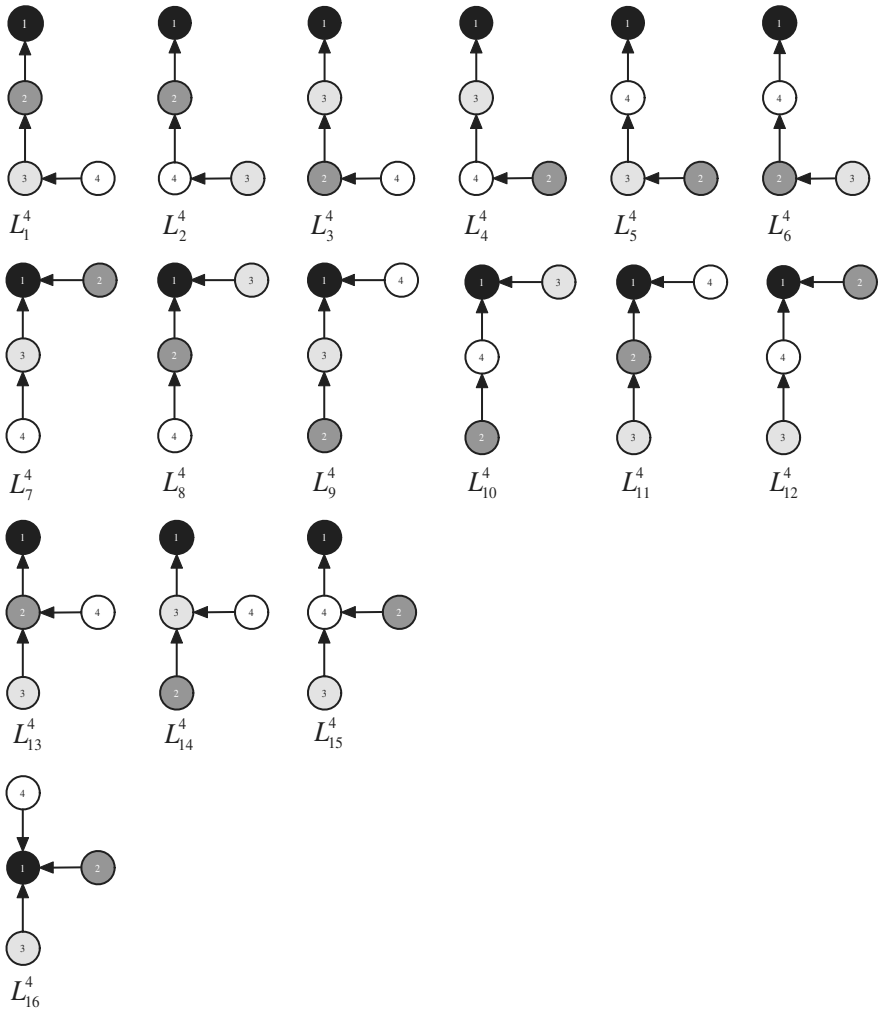

Fig. A1 Sixteen different spanning trees for a formation of four spacecraft.

$$(A_a)_{16} = \begin{bmatrix} \frac{-2v_1a_1^2}{\mu} & \frac{2v_2a_2^2}{\mu} & 0 & 0 \\ \frac{-2v_1a_1^2}{\mu} & 0 & \frac{2v_3a_3^2}{\mu} & 0 \\ \frac{-2v_1a_1^2}{\mu} & 0 & 0 & \frac{2v_4a_4^2}{\mu} \end{bmatrix}, \qquad \mathbf{b}_{16} = \begin{bmatrix} \Delta a_{2,1} \\ \Delta a_{3,1} \\ \Delta a_{4,1} \end{bmatrix} \tag{A5}$$

Substitution into Eq. (47) yields the optimal velocity-correction vector, which is equal for the four different trees already described, as is the final value of the semimajor axis of this formation (without perturbations):

$$\Delta\mathbf{v}^\star = \begin{bmatrix} 0.3826 \\ 0.1273 \\ 0.0180 \\ -0.5285 \end{bmatrix} \text{ m/s}, \qquad a^+ = a^\star = 42,170.49 \text{ km} \tag{A6}$$

This example shows that different spanning trees do not affect the control vector and the required velocity corrections of each spacecraft. This is because different spanning trees are merely a different parametrization of the same physical values of orbital elements. The final value of the orbital element is an optimal value for given initial conditions. Choosing different spanning trees does not change these initial values and the concomitant required corrections $\Delta\boldsymbol{\alpha}$.

Acknowledgments

This research was partially supported by the Israel Ministry of Science and Technology Infrastructure Program. The authors owe a debt of gratitude to Moshe Guelman and David Mishne for providing important insights.

References

[1] Clohessy, W., and Wiltshire, R., "Terminal Guidance System for Satellite Rendezvous," *Journal of the Astronautical Sciences*, Vol. 27, No. 9, 1960, pp. 653–678.

[2] Karlgaard, C. D., and Lutze, F. H., "Second-Order Relative Motion Equations," *Journal of Guidance, Control, and Dynamics*, Vol. 26, No. 1, Jan. 2003, pp. 41–49.

[3] Gurfil, P., and Kasdin, N. J., "Nonlinear Modeling of Spacecraft Relative Motion in the Configuration Space," *Journal of Guidance, Control, and Dynamics*, Vol. 27, No. 1, 2004, pp. 154–157. doi:10.2514/1.9343

[4] Chichka, D., "Satellite Clusters with Constant Apparent Distribution," *Journal of Guidance, Control, and Dynamics*, Vol. 24, No. 1, 2001, pp. 117–122.

[5] Alfriend, K., Schaub, H., and Gim, D., "Gravitational Pertubations, Nonlinearity and Circular Orbit Assumption Effects on Formation Flying Control Strategies," 23rd AAS Guidance and Control Conference, American Astronautical Society Paper AAS-00-012, 2000.

[6] Schaub, H., and Alfriend, T., "J_2 Invariant Relative Orbits for Spacecraft Formations," *Celestial Mechanics and Dynamical Astronomy*, Vol. 79, No. 2, 2001, pp. 77–95. doi:10.1023/A:1011161811472

[7] Schaub, H., Vadali, S. R., and Alfriend, K. T., "Spacecraft Formation Flying Control Using Mean Orbital Elements," *Journal of the Astronautical Sciences*, Vol. 48, No. 1, 2000, pp. 69–87.

[8] Mishne, D., "Formation Control of Satellites Subject to Drag Variations and J_2 Perturbations," *Journal of Guidance, Control, and Dynamics*, Vol. 27, No. 4, 2004, pp. 685–692. doi:10.2514/1.11156

[9] Schaub, H., and Alfriend, K., "Hybrid Cartesian and Orbit Elements Feedback Law for Formation Flying Spacecraft," *Journal of Guidance, Control, and Dynamics*, Vol. 25, No. 2, Mar.–Apr. 2002, pp. 387–393.

[10] Gurfil, P., "Relative Motion Between Elliptic Orbits: Generalized Boundedness Conditions and Optimal Formationkeeping," *Journal of Guidance, Control, and Dynamics*, Vol. 28, No. 4, July 2005, pp. 761–767.
doi:10.2514/1.9439

[11] Hughes, S. P., Cooley, D. S., and Guzman, J. J., "A Direct Approach for Minimum Fuel Maneuvers of Distributed Spacecraft in Multiple Flight Regimes," *Advances in the Astronautical Sciences*, Vol. 120, No. 1, 2005, pp. 869–898.

[12] Schaub, H., "Incorporating Secular Drifts into the Orbit Element Difference Description of Relative Orbits," *Advances in the Astronautical Sciences*, Vol. 114, 2003, pp. 239–257.

[13] Battin, R. H., *An Introduction to the Mathematics and Methods of Astrodynamics*, AIAA, Reston, VA, 1999, pp. 488–489, Chap. 10.

[14] Tillerson, M., Breger, L., and How, J. P., "Distributed Coordination and Control of Formation Flying Spacecraft," *Proceedings of the American Control Conference*, Vol. 2, American Automatic Control Council, Evanston, IL, 2003, pp. 1740–1745.

[15] Ross, I. M., King, J., and Fahroo, F., "Designing Optimal Spacecraft Formations," AIAA/AAS Astrodynamics Conference, AIAA Paper 2002-4635, Aug. 2002.

[16] Yang, G., Yang, Q., Kapila, V., Palmer, D., and Vaidyanathan, R., "Fuel Optimal Manoeuvres for Multiple Spacecraft Formation Reconfiguration Using Multi-Agent Optimization," *International Journal of Robust and Nonlinear Control*, Vol. 12, No. 3, 2002, pp. 243–283.
doi:10.1002/rnc.684

[17] Vadali, S. R., Vaddi, S. S., and Alfriend, K. T., "An Intelligent Control Concept for Formation Flying Satellites," *International Journal of Robust and Nonlinear Control*, Vol. 12, No. 3, Mar. 2002, pp. 97–115.
doi:10.1002/rnc.678

[18] Diestel, R., *Graph Theory*, Springer–Verlag, New York, 2005, pp. 1–30.

[19] Mesbahi, M., and Hadaegh, F., "Formation Flying Control of Multiple Spacecraft via Graphs, Matrix Inequalities, and Switching," *Journal of Guidance, Control, and Dynamics*, Vol. 24, No. 2, 2001, pp. 369–377.

[20] Vallado, D. A., *Fundamentals of Astrodynamics and Applications*, 2nd ed., 2001, pp. 135–235.

[21] Ross, I. M., "Space Trajectory Optimization and L_1-Optimal Control Problems," *Modern Astrodynamics*, edited by P. Gurfil, Elsevier, Amsterdam, 2006, pp. 155–188.

[22] Even, S., *Graph Algorithms*, Computer Science Press, New York, 1979, pp. 150–154.